STRUCTURAL AND MAGNETIC PHASE TRANSITIONS IN HEXAGONAL PEROVSKITES

IRAM MUNAWAR

NOTE TO USERS

Structural and Magnetic Phase Transitions in Hexagonal Perovskites

by

© Iram Munawar
M.Sc. (2000) University of the Punjab

A thesis submitted to the
School of Graduate Studies
in partial fulfillment of the
requirements for the degree of
Master of Science.

Department of Physics and Physical Oceanography
Memorial University of Newfoundland

September 20, 2004

ST. JOHN'S NEWFOUNDLAND

Your file Votre référence
ISBN: 0-494-02362-7
Our file Notre référence
ISBN: 0-494-02362-7

Contents

Abstract

The rare earth manganites $RMnO_3$ for R=Ho, Er, Yb crystallize in hexagonal perovskites type structures with symmetry $P6_3cm[\#185,(C_{6v}^3)]$. In this work, the structural and magnetic phase transitions are investigated by considering the Landau theory of phase transitions, in which the transition order parameter transforms according to the irreducible representations of the high symmetry space group. The structural phase transitions occurring at the Γ point for one component order parameters A_1, A_2, B_1 and B_2 lead to symmetries $P6_3cm$ (C_{6v}^3), $P6_3$ (C_6^6), P3c1 (C_{3v}^3) and P31m (C_{3v}^2) respectively. For the two component order parameter E_1, the low symmetry phases as a result of structural phase transitions are Pm (C_s^1) and Pc (C_s^2) corresponding to the equilibrium values (η,0), (0,η). For E_2, the two low symmetry phases correspond to the same symmetry group $Cmc2_1$ (C_{2v}^{12}) with opposite values of equilibrium order parameter i.e., (η,0), (-η,0).

The structural changes are also found at the M-point of the hexagonal Brillouin zone. The three-dimensional space group representations at the M-point are M_1, M_2, M_3 and M_4. The low symmetry phases appearing at M_1 are $P6_3cm$ (C_{6v}^3), $Cmc2_1$ (C_{2v}^{12}) and $Pmc2_1$ (C_{2v}^1). For M_2, the low symmetry phases are $P6_3$ (C_6^6), $Cmc2_1$ (C_{2v}^{12}) and $Pmn2_1$ (C_{2v}^7). For M_3, the low symmetry phases are P3c1 (C_{3v}^3), Cc (C_s^4) and Pc (C_s^2). For M_4, the low symmetry phases are P31m (C_{3v}^2), Cm (C_s^3) and Pm (C_s^1).

The magnetic symmetry of $RMnO_3$ as a result of magnetic ordering in R^{3+} ions is supposed to be Pc for $HoMnO_3$ and $P\underline{c}$ for $ErMnO_3$, $YbMnO_3$. The irreducible representation E_1 at the Γ point or M_3 representation at the M-point of the hexagonal Brillouin zone are proposed to be related to this symmetry for $HoMnO_3$.

Acknowledgements

All my thanks and gratitudes are for Almighty God Who has blessed me for rendering this work.

I feel highly thankful of my supervisor Dr. S. H. Curnoe for assigning me this job, her timely guidance, valuable advices and financial support.

I would like to thank Marek Bromberek for his help throughout my M.Sc program and Dr. Ivan Sergienko for his suggestions in my research work.

List of Tables

List of Figures

Chapter 1

Hexagonal Perovskites

Perovskite is the most abundant mineral on earth. It was first described in the 1830's by the geologist Gustav Rose, who named it after the famous Russian mineralogist Count Lev Aleksevich von Perovski. The principle perovskite structure, found in ferroelectric materials, is simple cubic, but perovskites also exist in hexagonal structures.

Most perovskites are dielectrics, but some of them are considered to be good conductors and semiconductors. The most common applications of the perovskites are as dielectric resonators ($BaZrO_3$), piezoelectric transducers ($Pb(Zr,Yi)O_3$), thick film resistors ($BaRuO_3$), electrostrictive actuators ($Pb(Mg,Nb)O_3$), laser hosts ($YAlO_3$), ferromagnets ($(Ca,La)MnO_3$), refractory electrodes ($LaCoO_3$), optical second harmonic generators ($KNbO_3$), multilayer capacitors ($BaTiO_3$) and $Ba(Pb,Bi)O_3$ superconductors layered cuprate.

The aim of the present work is to study the structural and magnetic phase transitions occurring in hexagonal perovskites $RMnO_3$ at the Γ point and the M-point of the hexagonal Brillouin zone. A group theoretical analysis is presented for these transitions on the basis of Landau theory of phase transitions, in which the transition

order parameter transforms according to an irreducible representation of the high symmetry space group. The Landau free energy has been expanded as a function of the order parameter components and the possible low symmetry phases are worked out.

1.1 Rare Earth and Yttrium Manganites

1.1.1 Overview of Materials

The rare earth and yttrium manganites $RMnO_3$ of the perovskites type structure have been known since the 1950's [1]. The compounds with larger ionic radius (R=La, Ce, Pr, Nd, Sm, Eu, Gd, Tb, Dy) crystallize in a perovskite structure with orthorhombic symmetry and belong to the space group Pnma[#62,(D_{2h}^{16})] [2]. The perovskite structure for material with smaller ionic radius (R = Ho, Er, Tm, Yb, Lu, Y and Sc) becomes metastable, and a new stabilized hexagonal phase with space group $P6_3cm$ [#185,(C_{6v}^{3})] appears [1]. The crystal structure of hexagonal $RMnO_3$ is shown in Figure 1.1.

The hexagonal rare earth and yttrium manganites have three lattice parameters a and c, plus an internal ε that represents the distance between oxygen and rare earth (yttrium) layers in units of c. The unit cell parameters of several hexagonal rare earth orthomanganites are shown in Table 1.1 [1].

The x-ray diffraction data on $RMnO_3$ compounds [1] indicate that there are six atoms per formula unit. The Wyckoff notations and atomic positions of these compounds are given in Table 1.2.

The rare earth and yttrium manganites can be converted into an orthorhombic configuration under high temperature and pressure [3, 4]. Pressure values exceed-

Compound	$a(\AA)$	$c(\AA)$	c/a
$YMnO_3$	6.125	11.41	1.862
$HoMnO_3$	6.136	11.42	1.861
$ErMnO_3$	6.115	11.41	1.866
$TmMnO_3$	6.062	11.40	1.881
$YbMnO_3$	6.062	11.40	1.881
$LuMnO_3$	6.042	11.37	1.882

Table 1.1: Unit cell parameters of rare earth orthomanganites. All a and c values are $\pm 0.001\AA$ and c/a values are ± 0.002.

Atoms	Wyckoff Notations	x	y	z
R(1)	4b	$\frac{1}{3}$	$\frac{2}{3}$	$\frac{1}{4}+\varepsilon$
R(2)	2a	0	0	$\frac{1}{4}-\varepsilon'$
Mn	6c	$\approx \frac{1}{3}$	0	0
O(1)	6c	$\approx \frac{1}{3}$	0	$\approx \frac{1}{6}$
O(2)	6c	$\approx \frac{2}{3}$	0	$\approx \frac{1}{3}$
O(3)	4b	$\frac{1}{3}$	$\frac{2}{3}$	≈ 0
O(4)	2a	0	0	$\approx \frac{1}{2}$

Table 1.2: Wyckoff notations and atomic positions for $RMnO_3$ compounds. The ε and ε' are approximately 0.02-0.03.

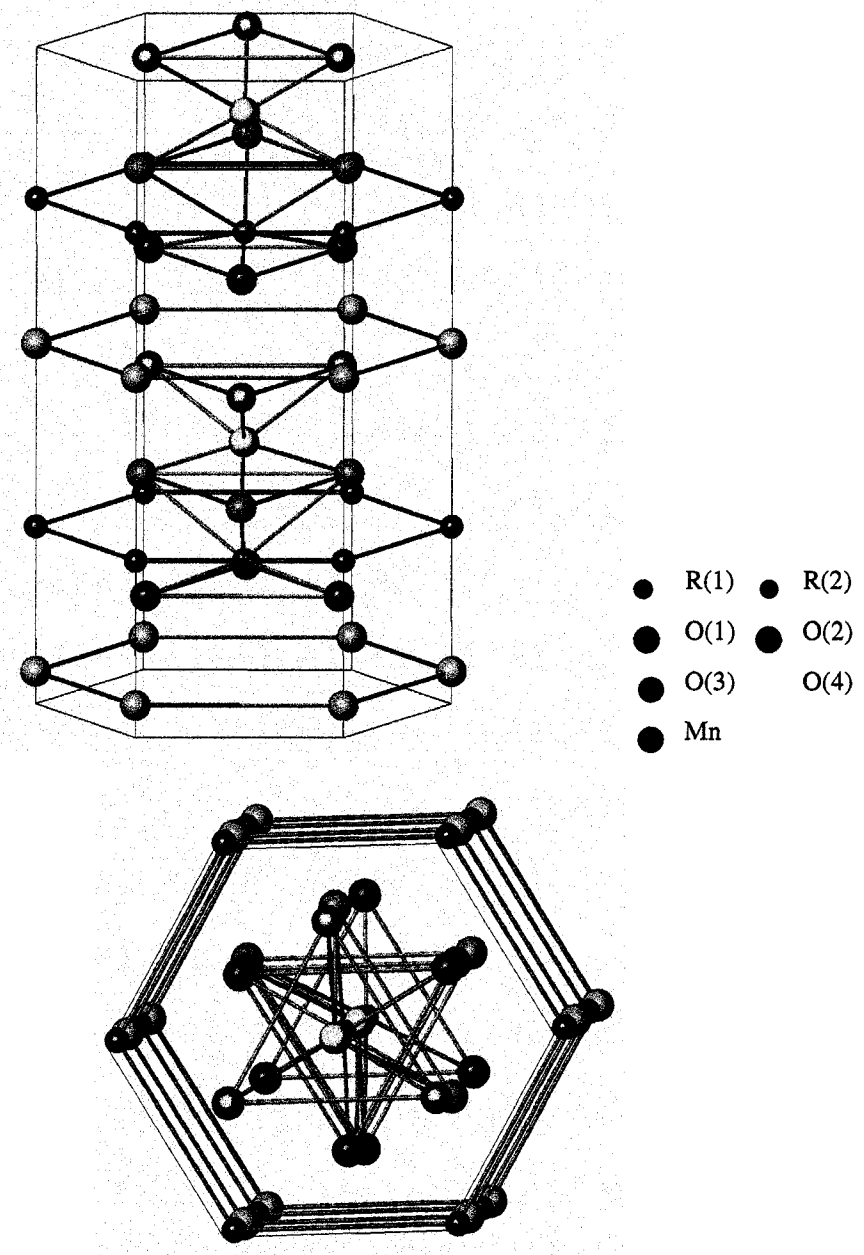

Figure 1.1: Crystal structure of hexagonal $RMnO_3$.

ing 35 kbar are necessary to transform hexagonal $YMnO_3$ and $HoMnO_3$ into an orthorhombic phase while the hexagonal $YbMnO_3$ transforms at a pressure of 40 kbar at 1000°C. X-ray diffraction studies indicate that both hexagonal and orthorhombic

forms do not undergo any other phase transitions. However, occasional traces of unreacted rare earth oxides have been found. The transformation from hexagonal to orthorhombic is reconstructive.

1.1.2 Γ Point Phonon Modes of $RMnO_3$

The group theoretical analysis for the Γ point phonon modes of hexagonal ($P6_3cm$) $RMnO_3$ is summarized in Table 1.3 [5]. From Table 1.3, one can see that out of a total of 60 Γ point modes ($10A_1+5A_2+10B_1+5B_2+15E_1+15E_2$), 38 are Raman active. Also the modes of A_1 and E_1 symmetries are infrared active while the modes of A_2, B_1 and B_2 symmetries are silent.

Atom	Site Symmetry	Irreducible Representation
R(1)	C_{3v}^v	$A_1+A_1+E_1+E_2$
R(2)	C_3	$A_1+A_2+B_1+B_2+2E_1+2E_2$
Mn	C_s^v	$2A_1+A_2+2B_1+B_2+3E_1+3E_2$
O(1)	C_s^v	$2A_1+A_2+2B_1+B_2+3E_1+3E_2$
O(2)	C_s^v	$2A_1+A_2+2B_1+B_2+3E_1+3E_2$
O(3)	C_{3v}^v	$A_1+B_1+E_1+E_2$
O(4)	C_3	$A_1+A_2+B_1+B_2+2E_1+2E_2$

Table 1.3: Atomic site symmetries and the irreducible representations in $RMnO_3$.

Modes Classification:

$\Gamma_{Raman} = 9A_1+14E_1+15E_2$

$\Gamma_{ir} = 9A_1+14E_1$

$\Gamma_{silent} = 5A_2+10B_1+5B_2$

$\Gamma_{acoustic} = A_1+E_1$

1.1.3 Ferroelectricity and Antiferromagnetism in $RMnO_3$

Recently, hexagonal manganites have attracted much attention because of the co-existence of ferroelectric and magnetic ordering. Ferroelectric ordering occurs at a very high temperature ($T_{FE} \approx 900$ K) while magnetic ordering occurs at a low temperature ($T_m \approx 100$ K). Therefore, the hexagonal yttrium and rare earth compounds form an interesting class of materials known as ferroelectromagnets [6]. In the past few years, experimental evidence of coupling between ferroelectric and magnetic ordering has been found. For instance, anomalies in the dielectric constant have been observed in $YMnO_3$ near its Néel temperature ($T_m \approx 80$ K) and below its ferroelectric Curie temperature ($T_{FE} \approx 914$ K). These anomalies indicate coupling between ferroelectric and antiferromagnetic ordering in $YMnO_3$, in spite of the large difference in two ordering temperatures [7–9]. Also a new re-entrant phase has been found in $HoMnO_3$ in the presence of a magnetic field less than 4.1 T below its zero-field Mn-spin orientation transition temperature of 32.8 K, showing a coupling between ferroelectric and magnetic orders [10–12]. $HoMnO_3$ shows ferroelectricity at $T_{FE} \approx 830$ K and antiferromagnetism developed at $T_m \approx 76$ K. The coupling between ferroelectric and magnetic order parameters allows for the manipulation of electrical properties through magnetic fields. This would then lead to the application of these compounds in the field of electronics.

This is not the case in the orthorhombic $RMnO_3$ compounds where only the magnetic ordering occurs but not the ferroelectric one [13]. The orthorhombic compounds display ferromagnetism, semiconductor-to-metal transitions, charge order and colossal magnetoresistance properties where as hexagonal compounds are poor conductors.

1.1.4 Magnetic Phase Transitions in $RMnO_3$

The magnetic ordering in hexagonal manganites $RMnO_3$ is due to Mn^{3+} sublattices and in some compounds R^{3+} sublattices, all of which are geometrically frustrated [14–17]. The magnetic phase diagram of $RMnO_3$ is analyzed by Faraday rotation (FR) and optical second harmonic generation (SHG). The Mn^{3+} ions at 6c positions, with local symmetry m, form a triangular lattice on the $z = 0$ and $z = c/2$ planes in the hexagonal unit cell. It has been investigated that in all compounds Mn^{3+} spins exhibit eight different types of triangular antiferromagnetic ordering in the basal plane. The magnetic structures of the Mn^{3+} sublattices in $RMnO_3$ are shown in Figure 1.2. The magnetic structures corresponding to four different types of magnetic ordering in Mn^{3+} sublattices are denoted by A_1, A_2, B_1, B_2 for the spin angle 0° or 90°, where spin angle is the angle between the Mn^{3+} magnetic moment and the x-axis. The symbols A_1, A_2, B_1, B_2 refers to the one-dimensional irreducible representations of the space group $P6_3cm$. When the spin angle is between 0° and 90° there are intermediate magnetic structures denoted as A, B, A_1' and A_2'.

The R^{3+} ions located at 2a and 4b positions, show ordering with a partially filled 4f shell. For instance, the Ho^{3+} sublattices shows antiferromagnetic or ferromagnetic ordering as given in Table 1.4.

According to published data [19] on the magnetic properties of $RMnO_3$ for R=Ho, Er, Yb, there exist two different phases with long range magnetic order at zero magnetic field in each manganite. These phases are denoted as Phase I for $ErMnO_3$ [20] and $YbMnO_3$ [14] or Phase I′ for $HoMnO_3$ [11, 21, 22] between T_{N1}=56 K–129 K and T_{N2}=4 K and Phase II for $ErMnO_3$ and $YbMnO_3$ or Phase II′ for $HoMnO_3$ below T_{N2}. The magnetic symmetry of Phase I is associated with the B_2 representation and corresponds to the magnetic space group $P\underline{6}_3\underline{c}m$ at $T_{N1} \approx 79$ K. The magnetic

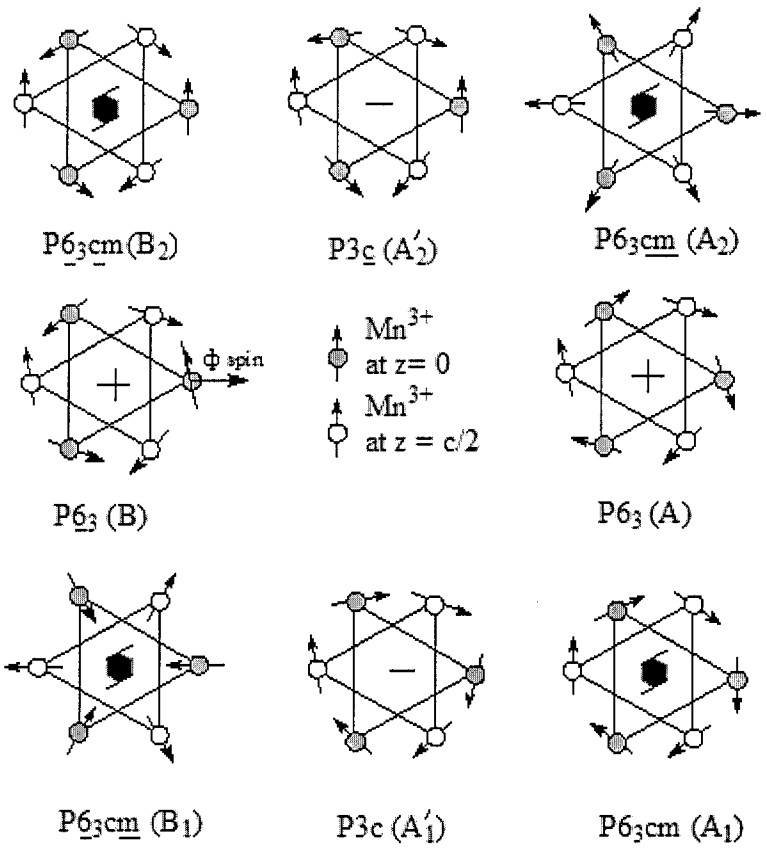

Figure 1.2: Magnetic ordering of Mn^{3+} sublattices. The drawings in each of the four corners correspond to the four one-dimensional irreducible representation A_1, A_2, B_1, B_2 of the space group $P6_3cm$, while the drawings in between them are intermediate structures A, B, A_1' and A_2' respectively. The magnetic space group corresponding to these symmetries are also shown (from Ref. [14]).

symmetry of Phase I′ is also associated with the B_2 representation with magnetic space group $P\underline{6_3}\underline{c}m$ at $T_{N1} \approx 76$ K. At $T_{N1} \approx 6$ K, the magnetic structure of Phase I′ is associated with the B_1 representation and has symmetry $P\underline{6_3}c\underline{m}$. It has also been observed in $HoMnO_3$ that a sharp Mn-spin-reorientation transition occurs in the low temperature range $T_{SR} \approx 33$ K that changes the magnetic symmetry from $P\underline{6_3}\underline{c}m$ to $P\underline{6_3}c\underline{m}$ (Phase I to Phase I′) [11].

Magnetic Symmetry	Ho(total)	Ho(2a) along z	Ho(2a) xy-plane	Ho(4b) along z	Ho(4b) xy-plane
$P\underline{6_3}\underline{c}m$	AFM	0	0	FM	AFM
$P\underline{6_3}c\underline{m}$	AFM	AFM	FM	AFM	FM
$P6_3cm$	AFM	0	0	AFM	AFM
$P6_3\underline{cm}$	FM	FM	FM	FM	FM

Table 1.4: Magnetic symmetry of Ho^{3+} sublattices (from Ref. [18]).

At low temperatures, the magnetic structure of $YbMnO_3$ changes from $P\underline{6_3}\underline{c}m$ to $P6_3\underline{cm}$ at 6 K, which corresponds to the A_2 representation. Also a transition takes place from $P\underline{6_3}$ to $P6_3$ in $ErMnO_3$ and $HoMnO_3$ below 5 K.

In $YMnO_3$, the Mn^{3+} sublattices orders antiferromagnetically below $T_{N1} \approx 79$ K. The corresponding magnetic structure transforms like B_1 and has symmetry $P\underline{6_3}c\underline{m}$, which exactly resembles to that of $HoMnO_3$ in the low temperature range [23–27].

There are indications [19] of a second order phase transition in $ErMnO_3$, $YbMnO_3$ and $HoMnO_3$ at T_{N2}, below which the magnetic long range order of rare earth R^{3+} ions develops. The magnetic symmetry of Phase II is $P\underline{c}$, which is a subgroup of the symmetry group of the high temperature phase. There is not any definite conclusion about the symmetry of Phase II′; however symmetry consideration and the results on spontaneous polarization indicate that the symmetry is Pc. The hexagonal $YMnO_3$ does not display long range ordering of R^{3+} ions because of the absence of a partially filled 4f shell. Therefore yttrium ions are non magnetic in this compounds.

1.2 Hexagonal Perovskites of ABX_3 Family

1.2.1 Overview of Materials

A great number of compounds with chemical formula ABX_3 crystallize in a hexagonal structure. Most of these compounds possess the high symmetry space group $P6_3/mmc$ [#194,(D^4_{6h})] [28]. The crystal structure of hexagonal $BaTiO_3$ (ABX_3 family) is shown in Figure 1.3. The transition temperatures and space groups of most of the ABX_3 compounds are listed in Table 1.5.

The atomic parameters of $BaTiO_3$, measured by using the powder diffraction technique, and the group theoretical analysis for the Γ point phonon modes of hexagonal ABX_3 are summarized in Table 1.6 and Table 1.7 respectively.

1.2.2 Structural and Magnetic Phase transitions in ABX_3

The hexagonal perovskites of the ABX_3 family undergo structural phase transitions by the condensation of one or several vibration modes. Various types of distortions have been found in different compounds. The Landau theory of phase transitions has been widely used in order to understand the mechanism of these transitions in crystals. The change in the symmetry of a crystal in the case of Landau type transitions can be described in terms of a symmetry-breaking order parameter, which transforms according to a physically irreducible representation (IR) of the high symmetry group. Perez-Mato *et al.* [32] have determined all the possible low symmetry phases derived from $P6_3/mmc$. The possible structural phase transitions of the Landau type in ABX_3 compounds occuring at the Γ point of a hexagonal Brillouin zone are listed in Table 1.7.

These materials also display magnetic phase transitions. The magnetic structure

Compound	Prototype Space Group	Low Symmetry Space Group
$KNiCl_3$	$P6_3/mmc$(762K)	$P6_3/cm$(561K) and $Pca2_1$ or Pbcm(274K)
$RbMnCl_3$	$P6_3/mmc$	$P2_1m$(272K)
$RbFeBr_3$	$P6_3/mmc$(713K)	$P6_3cm$(108K)
$RbVBr_3$	$P6_3/mmc$(1263K)	$P6_3cm$ or P3′c1(90K)
$RbCrBr_3$	$P6_3/mmc$	C2(184K) and C2/m(Unknown)
$RbMnBr_3$	$P6_3/mmc$(725K)	$P6_3cm$(470K)
$RbMgBr_3$	$P6_3/mmc$(738K)	P3′c1(449K)
$RbNiCl_3$	$P6_3/mmc$	—
$RbMgH_3$	$P6_3/mmc$	—
$RbCoBr_3$	$P6_3/mmc$	—
$CsCoBr_3$	$P6_3/mmc$	—
$CsNiCl_3$	$P6_3/mmc$	—
$CsCoCl_3$	$P6_3/mmc$	—
$CsMnBr_3$	$P6_3/mmc$	—
$CsMnI_3$	$P6_3/mmc$	—
$SrMnO_3$	$P6_3/mmc$	—
$BaMnO_3$	$P6_3/mmc$	—
$BaTiO_3$	$P6_3/mmc$(300K)	$C222_1$(222K) and $Cmc2_1$ or $P2_1$(74K)
$BaVS_3$	$P6_3/mmc$	—
$BaRuO_3$	$P6_3/mmc$	—
$TlFeCl_3$	$P6_3/mmc$	—

Table 1.5: The transition temperatures and space groups for ABX_3.

Atoms	Wyckoff Notations	x	y	z
Ba(1)	4f	$\frac{1}{3}$	$\frac{1}{6}$	0.09615(7)
Ba(2)	2b	0	0	$\frac{1}{4}$
Ti(1)	4f	$\frac{1}{3}$	$\frac{1}{6}$	0.84794(11)
Ti(2)	2a	0	0	0
O(1)	12k	0.83400(7)	0.66800(14)	0.08094(3)
O(2)	6h	0.51749(8)	0.03504(17)	$\frac{1}{4}$

Table 1.6: Wyckoff Notations and atomic positions for $BaTiO_3$ [29].

Atoms	Site Symmetry	Irreducible Representations
A(1)	C_{3v}^d	$A_{1g}+A_{2u}+B_{1g}+B_{2u}+E_{1g}+E_{1u}+E_{2g}+E_{2u}$
A(2)	D_{3h}^1	$A_{2u}+B_{1g}+E_{1u}+E_{2g}$
B(1)	C_{3v}^d	$A_{1g}+A_{2u}+B_{1g}+B_{2u}+E_{1g}+E_{1u}+E_{2g}+E_{2u}$
B(2)	D_{3d}	$A_{2u}+B_{2u}+E_{1u}+E_{2u}$
X(1)	C_s^d	$2A_{1g}+A_{1u}+A_{2g}+2A_{2u}+2B_{1g}+B_{1u}+B_{2g}+2B_{2u}$ $+3E_{1g}+3E_{1u}+3E_{2g}+3E_{2u}$
X(2)	C_{2v}^1	$A_{1g}+A_{2g}+A_{2u}+B_{1g}+B_{1u}+B_{2u}+E_{1g}+2E_{1u}+2E_{2g}+E_{2u}$

Table 1.7: Atomic site symmetries and the irreducible representations in ABX_3 [5].

Point on h-BZ	Irreducible Representations	Order Parameter Space	Space Group
Γ	A_{2g}	—	$P6_3/m$ (C_{6h}^2)
	B_{1g}	—	$P\bar{3}1c$ (D_{3d}^2)
	B_{2g}	—	$P\bar{3}m1$ (D_{3d}^3)
	A_{1u}	—	$P6_322$ (D_6^6)
	A_{2u}	—	$P6_3mc$ (C_{6v}^4)
	B_{1u}	—	$P\bar{6}m2$ (D_{3h}^1)
	B_{2u}	—	$P\bar{6}2c$ (D_{3h}^4)
	E_{1g}	$(0\ \eta)$	$C2/m$ (C_{2h}^3)
		$(\eta\ 0)$	$B2/b$ (C_{2h}^6)
		$(\eta_1\ \eta_2)$	$P\bar{1}$ (C_i^1)
	E_{2g}	$(\eta\ 0)$	$Cmcm$ (D_{2h}^{17})
		$(\eta_1\ \eta_2)$	$P2_1/m$ (C_{2h}^2)
	E_{1u}	$(\eta\ 0)$	$Amm2$ (C_{2v}^{14})
		$(0\ \eta)$	$Ama2$ (C_{2v}^{16})
		$(\eta_1\ \eta_2)$	Pm (C_{1h}^1)
	E_{2u}	$(0\ \eta)$	$Cmc2_1$ (C_{2v}^{12})
		$(\eta\ 0)$	$C222_1$ (D_2^5)
		$(\eta_1\ \eta_2)$	$P2_1$ (C_2^2)

Table 1.8: Structural phase transitions for IR at Γ point in a crystal with $P6_3/mmc$ symmetry [32].

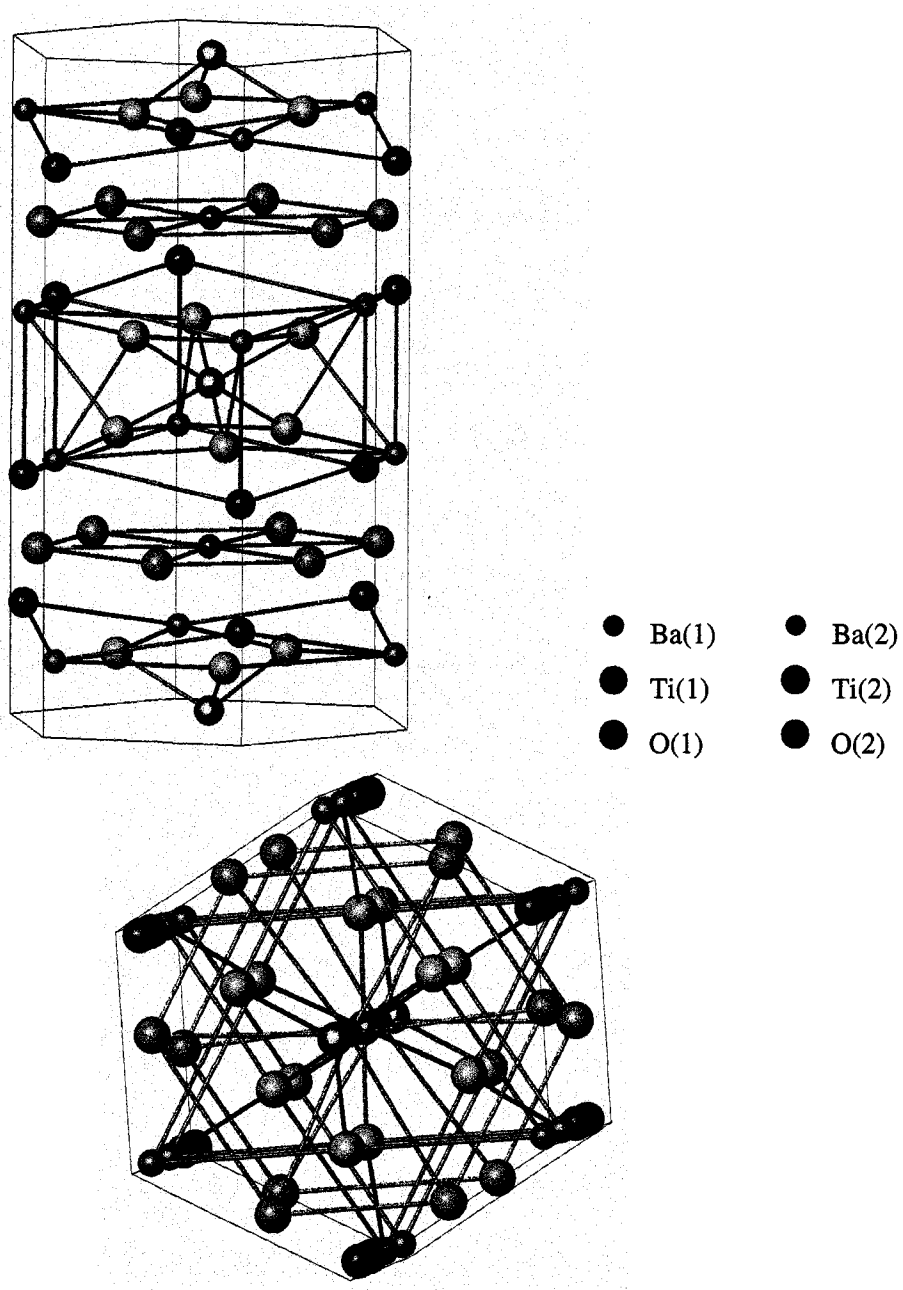

Figure 1.3: Crystal structure of hexagonal $BaTiO_3$.

of the ABX_3 family of hexagonal perovskites is normally triangular or close to triangular. On the basis of structural and magnetic properties, some of the ABX_3 family compounds can be grouped into three classes. Class I includes $KNiCl_3$, $RbMnBr_3$

and $TlFeCl_3$ that undergo structural phase transitions at temperatures higher than their magnetic ordering points. The intermediate phases show ferroelectricity that disappears in the lowest temperature range. The Class II compound $RbFeBr_3$, shows both ferroelectricity and antiferromagnetism at the lowest temperature phase. In Class III, the compounds $RbCoBr_3$ and $RbVBr_3$ display dielectric anomalies around a magnetic ordering temperature region [38].

1.2.3 Structural Phase Transitions in $KNiCl_3$

$KNiCl_3$ crystallizes into a high symmetry space group $P6_3/mmc$ (D^4_{6h}) [30]. Recent dielectric studies of $KNiCl_3$ indicate structural phase transitions at 274 K, 285 K, 561 K and 762 K. The structural phase transition at room temperature (561 K) corresponds to the space group $P6_3cm$ (C^3_{6v}) [31]. A K_4 mode at the point K=($-\frac{1}{3}$ $\frac{2}{3}$ 0) of the hexagonal Brillouin zone is proposed to be responsible for this symmetry [32–35]. The structural phase transition from $P6_3/mmc$ to $P6_3cm$ is of second order and is determined by Landau theory. Also there are two successive structural phase transitions at 285 K and 274 K. The structural phase transition at 285 K does not differ much from the structural phase transition at room temperature. The phase transition at 274 K changes the symmetry from hexagonal to orthorhombic. The phase transition from hexagonal to orthorhombic is a first order phase transition. The possible space group for the orthorhombic phase is thought to be $Pca2_1$ or Pbcm. A schematic diagram of the structural phase transitions occurring in $KNiCl_3$ at different temperature ranges is shown in Figure 1.4. The same type of distortions have also been found in $RbMnBr_3$.

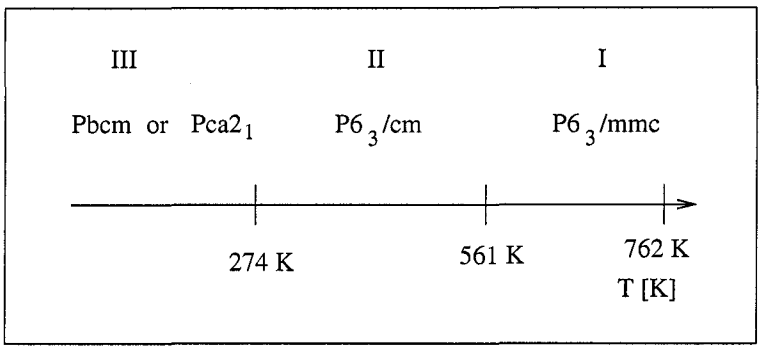

Figure 1.4: Schematic diagram of the structural phase transitions in $KNiCl_3$.

1.2.4 Landau Theory of Structural Phase Transitions in $BaTiO_3$

Hexagonal barium titanate (h-$BaTiO_3$, space group $P6_3/mmc$ at room temperature) undergoes two structural phase transitions at T_0= 222 K and T_c=74 K [39–41]. The origin of the transition at T_0 occurs as a result of the destabilization of a non-polar soft optic phonon E_{2u} of the high temperature phase (Phase I) with space group ($P6_3/mmc$)[42–45]. Phase II following the transition is orthorhombic and belongs to the space group $C222_1(D_2^5)$. With further decrease in temperature, a ferroelectric phase transition occurs at T_c, and both ferroelectric and ferroelastic properties are exhibited below T_c (Phase III). There are two possibilities for the space group of Phase III, $Cmc2_1$ or $P2_1$ [46, 47]. A schematic diagram of structural phase transitions in $BaTiO_3$ at different temperature ranges is shown in Figure 1.5. The phase transitions in hexagonal $BaTiO_3$ are discussed by considering Landau-type free energy functionals with emphasis on the transition between Phase II and Phase III. For this, the expression for the free energy [48] can be written in terms of order parameter (η_1, η_2), which transforms as the bases of the E_{2u} representation. i.e., $((x^2-y^2)z/2, xyz)$

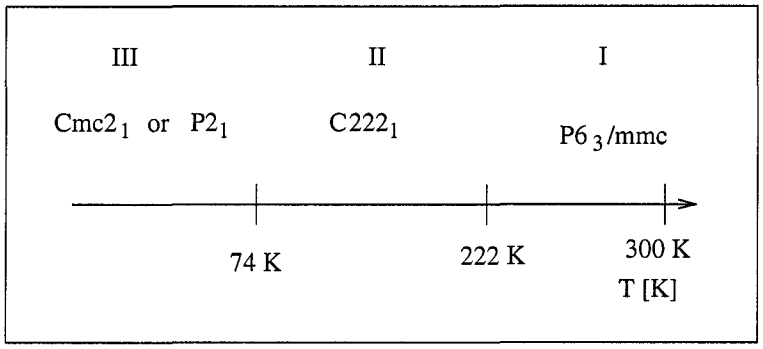

Figure 1.5: Schematic diagram of structural phase transitions in $BaTiO_3$.

as:

$$\begin{aligned} F &= \tfrac{\alpha}{2}(\eta_1^2+\eta_2^2)+\tfrac{\beta}{4}(\eta_1^2+\eta_2^2)^2+\tfrac{\gamma_1}{6}(\eta_1^2+\eta_2^2)^3+\tfrac{\gamma_2}{6}\eta_1^2(\eta_1^2-3\eta_2^2)^2+\tfrac{\varepsilon_1}{8}(\eta_1^2+\eta_2^2)^4 \\ &+ \tfrac{\varepsilon_2}{8}\eta_1^2(\eta_1^2-3\eta_2^2)^2(\eta_1^2+\eta_2^2)+\tfrac{c_{11}}{2}(u_1^2+u_2^2)+c_{12}u_1u_2+\tfrac{c_{66}}{2}u_6^2 \\ &+ \delta_1(u_1+u_2)(\eta_1^2+\eta_2)+\delta[(u_1-u_2)(\eta_1^2-\eta_2)-2u_6\eta_1\eta_2]+\tfrac{P_3^2}{2\chi} \\ &+ \zeta P_3\eta_1(\eta_1^2-3\eta_2^2)+\eta P_3[(u_1-u_2)\eta_1+u_6\eta_2]+\ldots., \end{aligned} \tag{1.1}$$

where P_i and u_i are the components of polarization and strain respectively. The coefficient α is temperature dependent, i.e., α=a(T-T_0).

According to phenomenological theory, eighth order terms are required for the transition from $C222_1$ to $Cmc2_1$, while the transition from $C222_1$ to $P2_1$ needs twelfth order terms in the Landau free energy. Also the transition from Phase II to $P2_1$ is of second order while the transition from Phase II to $Cmc2_1$ cannot be of second order.

Moreover, it has been investigated that a polar soft optic phonon with A_{2u} symmetry, independent of non-polar soft optic phonon with E_{2u} symmetry, induces a phase transition at T_0. This lowest frequency polar soft phonon A_{2u} splits into two peaks below T_0, which is unusual because it belongs to the one-dimensional representation. However, it is possible that the polar soft mode A_{2u} couples with another non-polar optic mode E_{2g} if this non-polar optic mode has a frequency very close to that of A_{2u}

mode above T_o [43]. This is because both A_{2u} and E_{2g}-modes belong to the same B_1 representation of the orthorhombic $C222_1$ below T_0 [49].

Chapter 2

Group Theory and Landau Theory

2.1 Group Theory

Group theory is one of the most powerful mathematical tools used in science, especially in physics and crystallography. It is the study of the algebra of transformations and symmetry and consists of elements and some binary operations such that: (i) closure: if a and b are in a group then $a.b$ is also in a group, (ii) associativity: if a, b, and c are in a group then $(a.b).c = a.(b.c)$, (iii) identity: an element e of the group such that for any element a of the group $a.e = e.a = a$, (iv) inverse: for any elements a of the group there is an a^{-1} such that $a.a^{-1} = a^{-1}$.a=e. Thus any system satisfying these four rules can be studied under group theory. The crystallographic groups such as point groups, space groups etc of a crystal can be identified by using group theory. Below is some description of these groups.

2.1.1 Point Groups

A point group is a group of symmetry operations which act at a point, including rotations, reflections and inversion [50]. The word "point" emphasizes the fact that

all the symmetry operations must act at one common point. This point is called the origin. The word "group" refers to the set of symmetry operations that form a group in a mathematical sense. There are 32 point groups. The list of these point groups is given in the Table 2.1.

A. Classification of Point Groups

The point groups can be classified into cyclic, dihedral, symmetric, tetrahedral and octahedral groups denoted by C, D, S, T and O respectively. Each of these classes is subdivided into different point groups. Here is a brief description about these point groups [51]. The notations used below are Schoenflies notation.

(i) The point groups in the class C are C_s, C_i, C_n, C_{nv} and C_{nh}, where n is an integer.

C_s: The point group C_s has a plane of symmetry and nothing more.

C_i: It contains only two symmetry operations, identity (E) and inversion (i) through a center of symmetry.

C_n: These groups contain only one axis of rotation. These are cyclic Abelian groups of order n.

C_{nv}: It contains a σ_v reflection in addition to the C_n axis.

C_{nh}: It contains a σ_h reflection in addition to the C_n axis.

(ii) The dihedral point group is defined by having a C_2 axis perpendicular to the principal C_n axis or there are nC_2's perpendicular to the C_n. The point groups in the class D are D_n, D_{nd} and D_{nh}, where n is an integer.

D_n: These groups have an n-fold rotation axis plus a two fold axis perpendicular to that axis.

D_{nh}: These groups contain the elements of D_n as well as horizontal reflection planes σ_h.

System	Label	Point Group	Number of Symmetry Elements
Triclinic	1	C_1	1
	$\bar{1}$	$C_i(S_2)$	2
Monoclinic	2	C_2	2
	m	C_s (C_{14})	2
	2/m	C_{2h}	4
Orthorhombic	222	D_2	4
	mm2	C_{2v}	4
	mmm	D_{2h}	8
Tetragonal	4	C_4	4
	$\bar{4}$	S_4	4
	4/m	C_{4h}	8
	422	D_4	8
	4mm	C_{4v}	8
	$\bar{4}$2m	D_{2d}	8
	4/mmm	D_{44}	16
Trigonal	3	C_3	3
	$\bar{3}$	$S_6(C_{3i})$	6
	32	D_3	6
	3m	C_{3v}	6
	$\bar{3}$m	D_{3d}	12
Hexagonal	6	C_6	6
	$\bar{6}$	C_{3h}	6
	6/m	C_{6h}	12
	622	D_6	12
	6mm	C_{6v}	12
	$\bar{6}$2m	D_{3h}	12
	6/mmm	D_{64}	24
Cubic	23	T	12
	m3	T_h	24
	432	O	24
	$\bar{4}$3m	T_d	24
	m3m	O_h	48

Table 2.1: List of 32 point groups [51].

D_{nd}: These groups are defined by the elements of D_n plus diagonal reflection planes σ_d bisecting the angle between the two fold axes perpendicular to the principal rotation axis.

(iii) The point groups in the class S are S_n, where n is an even integer. They contain a S_n axis plus a $C_{\frac{n}{2}}$ axis coinciding with it.

(iv) The tetrahedral group consists of T, T_d and T_h.

T: It is the smallest group of higher symmetry and contains four C_3 axes and three C_2 axes in addition to identity element.

T_d: It consists of 24 symmetry elements and has three planes of symmetry that contain the C_3 axes. The point groupT is a subgroup of T_d.

T_h: It also consists of 24 symmetry elements and has six planes of symmetry that contain the C_3 axes. It is a direct product of T with the inversion symmetry.

(v) The point group in the octahedral class O and O_h.

O: This is a group of proper rotations that transform a cube into itself. It has 24 symmetry elements.

O_h: It is the group of second highest symmetry including improper rotations and reflections and has 48 symmetry elements.

B. Symmetry Operations of Point Groups

The notations of the symmetry operations which appear in point groups include identity E, clockwise rotation C_n through an angle of 2π/n radians, where n=1,2,3,4,6, an improper clockwise rotation S_n through an angle of 2π/n radians (it is a symmetry operation corresponding to a rotation followed by an inversion operation), inversion operator ι (S_2), mirror plane σ, horizontal reflection plane σ_h that passes through the origin and perpendicular to the axis with the highest symmetry, vertical reflection plane σ_v which passes through the origin and the axis with the highest symmetry

and diagonal reflection plane σ_d through the origin and the axis with the highest symmetry but also bisecting the angle between the two fold axes perpendicular to the symmetry axis.

C. Representations and Character Tables of Point Groups

A representation of a group is a set of matrices having the same multiplication table as the group and can be written as $R(A)$, where R is the matrix to represent symmetry operation A. The number of rows and columns in the matrix determine the dimensionality of the representation. If there are two representations of a group $R^1(A)$ and $R^2(A)$, one can construct a new representation by combining their matrices i.e.,

$$R^3(A) = \begin{pmatrix} R^1(A) & 0 \\ 0 & R^2(A) \end{pmatrix} \tag{2.1}$$

Here the dimension of the matrix $R^3(A)$ is equal to the sum of the dimensions of $R^1(A)$ and $R^2(A)$. In (2.1), the matrices $R^1(A)$ and $R^2(A)$ appear in the upper left-hand and lower right-hand corners respectively, while the rest of the elements are zero. Any representation, whose elements appear in this form, is called the reducible representation. But if there does not exist any unitary transformation that can bring every matrix in a representation into this block diagonal form, then the representation is said to be irreducible representation. The irreducible representations are of fundamental importance in group theory.

Character table is associated with each point group and contains all information in a compact form that is necessary in dealing with point groups. The word "character" refers to the trace of a matrix. The various irreducible representations (IR) are collected in character tables. The notation used for IR's were developed by R. S. Mulliken [52]. In this notation, A and B denote one-dimensional representation, E

denotes two dimensional representations, T denotes three-dimensional representation. Furthermore, subscripts 1,2..., prime and double primes are used for distinction. The symmetries with inversion are assigned by subscripts g and u after the German words "gerade" (even) and "ungerade" (odd). The last two columns in a character table shows the first order and second order combinations of Cartesian coordinates.

2.1.2 Space Groups

The space group of the crystal is a combination of all available point group symmetry operations with the Bravais lattice translations, or one can say that the collection of all symmetry operations that take a crystal into itself is called the space group of the crystal. There are 230 space groups made from the combination of 32 point groups with the 14 Bravias lattices which belong to one of 7 crystal systems [53]. The notations, symmetry elements or general position etc of all the 230 space groups are given in *International Tables of X-Ray Crystallography* [54]. The space group symmetry operations may contain translations followed by rotation or reflection. These types of symmetry operations are known as screw rotations or glide reflections. Therefore, space groups are divided into groups known as symmorphic space group and non-symmorphic space groups [55]. The symmorphic space groups are the one which are generated without using glide planes or screw axes. There are 73 symmorphic space groups. The non-symmorphic space groups involve glide planes and/or screw rotations.

In order to work out the IR's of a space group [56–58], it is necessary to consider the lattice in k space and the corresponding Brillouin zone. After constructing Brillouin zone in k space, one needs to choose a $\mathbf{k}$ vector in or on the surface of the Brillouin zone. By applying all the symmetry operations of the point group on the $\mathbf{k}$ vector, one

can determine the "little group" and k*. The little group consists of the symmetry operations that leave **k** vector invariant, while k* is the set of **k** vectors found by applying all symmetry operations to **k**. The dimension of the IR of the space group is a product of dimension of IR of the little group and number of vectors in the k*. Thus by specifying the IR's of the little group, one can determine the IR's of the entire space group. The space group IR's at the Γ point of the Brillouin zone are the same as the point group IR's.

2.1.3 Magnetic Point Groups and Space Groups

The magnetic point groups were first studied by Shubnikov [59] and are generated by defining an extra coordinate in addition to the ordinary position coordinate (x, y, z) in a crystal. This extra coordinate takes only two possible values, referred to as color (black or white), sign (+ or -), or magnetic moment (parallel or antiparallel) and is known as operation of anti-symmetry, denoted by $\Re$. In this type of crystallography a general point is represented in four dimensions, namely, (x, y, z, s), where s refers to the extra coordinate and takes a value of +1 or -1. By considering the operation of anti-symmetry $\Re$, one can generate 58 magnetic point groups and 1191 magnetic space groups. Also the inclusion of $\Re$ with "all white" groups and the "grey" groups leads to 122 point groups and 1651 space groups [53].

The magnetic point groups can be categorized into three types. Type I includes ordinary 32 point groups. These point groups do not have anti-symmetry operation $\Re$. Type II includes 32 "grey" point groups, which appear if every equivalent site has both a white colored object and black colored object so that the overall color becomes grey. Thus in this case the operation of anti-symmetry $\Re$ is an operation of the group and has the effect of doubling the size of the original point group. A

general coordinate is $(x, y, z, \pm s)$. Type III includes 58 black and white or magnetic point groups. In this case the operation of anti-symmetry $\Re$ is not an element of the group independently, but half of the elements of the group are multiplied by $\Re$ while the other half form a subgroup on their own known the halving group.

The magnetic space groups can be divided into four types. Type I are the ordinary 230 space groups. Type II include 230 grey space groups, which are Type I space groups with time reversal. Type III includes 674 black and white space groups based on ordinary Bravais lattice and Type IV includes 517 black and white space groups based on black and white Bravais lattice. In addition to the 14 ordinary Bravais lattice, there are 22 black and white Bravais lattices [53].

2.2 Landau Theory of Phase Transitions

The Landau theory of continuous phase transitions was proposed by the Russian physicist L. D. Landau in 1937 [60–62]. It is a macroscopic theory that can be used to study several important features of structural phase transitions. For instance, the dimension and symmetry properties of the transition's order parameter, the form of free energy expansion and the change in crystal's space groups and point groups. It is based on a power series expansion of the excess free energy that the low temperature phase possesses relative to the high temperature phase and has the following form for a one-dimensional order parameter:

$$F(T, P, \eta) = F_o(T, P) + A\eta + \tfrac{\alpha}{2}\eta^2 + \tfrac{\beta}{3}\eta^3 + \tfrac{\gamma}{4}\eta^4 + ... \tag{2.2}$$

where η is an order parameter describing the changes in a symmetry of a crystal and the coefficients α, β, γ depends on the mechanical or electrical properties of the material and are functions of pressure and temperature.

By considering Landau expansion to fourth order and minimizing F for equilibrium, one gets:

$$\frac{\partial F}{\partial \eta} = A + \alpha\eta + \beta\eta^2 + \gamma\eta^3 = 0, \tag{2.3}$$

$$\frac{\partial^2 F}{\partial \eta^2} = \alpha + 2\beta\eta + 3\gamma\eta^2 \geq 0. \tag{2.4}$$

The three solutions of η are: η_I=0 and $\eta_{II} = [-\beta \pm (\beta^2 - 4\alpha\gamma)^{1/2}]/2\gamma$. It has been assumed that the states for η=0 and $\eta \neq 0$ are of different symmetry so the first term A in (2.1) becomes zero. The high temperature phase (above transition) for T>T_c, η=0 correspond to the minimum of F only if $\alpha > 0$. In the low temperature phase (below the transition) for T<T_c, the non zero value of η correspond to the minimum of F for $\alpha < 0$. These situations are shown in a Fig 2.1.

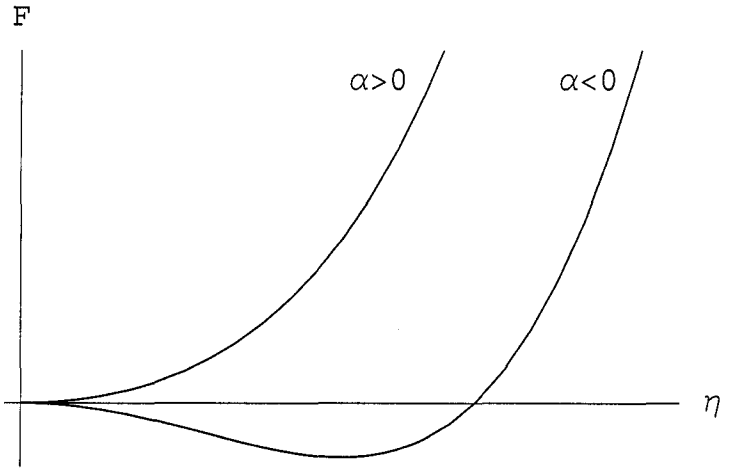

Figure 2.1: The plot of F versus η for $\alpha < 0$ and $\alpha > 0$.

Also $\eta > 0$ in the low temperature phase requires β and γ both positive by keeping α negative, which is possible only if $\alpha = a(T - T_c)$, where a is a positive constant and the other coefficients are independent of temperature. So (2.1) becomes:

$$F(T, P, \eta) = F_o(T, P) + \frac{a(T-T_c)}{2}\eta^2 + \frac{\beta}{3}\eta^3 + \frac{\gamma}{4}\eta^4. \tag{2.5}$$

However, at the transition temperature T_c, the minimization condition:

$$\frac{\partial F}{\partial \eta} = a(T - T_c)\eta + \beta\eta^2 + \gamma\eta^3 = 0. \quad (2.6)$$

requires $\beta\eta^2+\gamma\eta^3=0$ and has two solutions at the transition temperature $\eta_I=0$ and $\eta_{II}=-\beta/\gamma$.

In order for η to be continuous through the transition, β must be zero. If however, β is not zero then the continuous phase transition can occur only at isolated points [63]. Thus by taking $\beta=0$ for continuous transition, the Landau free energy to fourth order becomes:

$$F(T, P, \eta) = F_o(T, P) + \frac{a(T-T_c)}{2}\eta^2 + \frac{\gamma}{4}\eta^4. \quad (2.7)$$

By minimizing F, one gets $\eta=0$ and $\eta=\pm\sqrt{\frac{a(T-T_c)}{\gamma}}$ showing that the order parameter possess a square root dependence as a function of temperature. The plot of F versus η is shown in Fig 2.2, one can see two minima corresponding to the same value of the free energy but opposite value of η.

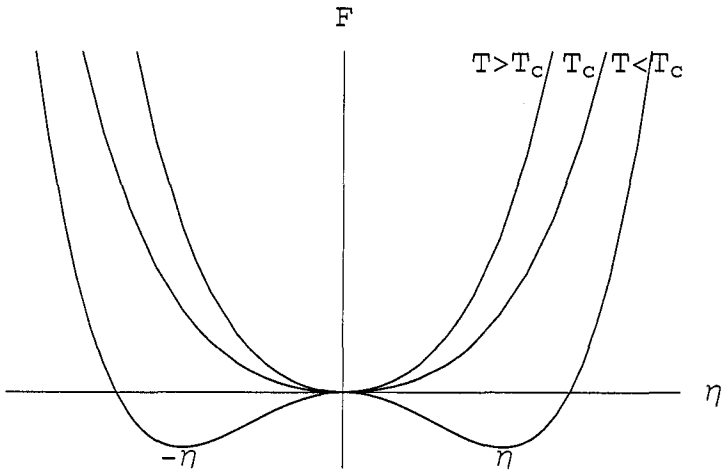

Figure 2.2: The plot of F versus η for three characteristic temperatures.

The Landau theory of continuous transitions has been used widely to describe the phenomena of ferroelastic and nonferroelastic phase transitions in crystals. The non-

ferroic phase transitions are defined as the structural phase transitions that appear by breaking the translational symmetry within the same crystal and do not involve the reduction of any point symmetry. A group theoretical analysis based on Landau theory for the free energy expansion and changes in a space group of a crystal in case of non-ferroic transitions has been developed [67].The ferroelectric and ferroelastic transitions involve the modification of the crystal's point group caused by the symmetry breaking of macroscopic quantities i.e., polarization, strain. A group theoretical analysis of these phase transitions based on Landau theory for the free energy expansion and changes in a point group and space group of a crystal has been done [64–66]. Gufan and his co-workers [68–72] discussed the free energy and phase diagram corresponding to the group generated by reflections C_{nv}, the cyclic group C_n and the cubic groups. Toledano *et al.* [73] summarized the free energy and phase diagram for C_1, C_{4v}, C_4, C_{3v}, C_3, O_h, T_h, O, T_d and T.

Chapter 3

Results and Discussion

Hexagonal rare earth manganites $RMnO_3$ (R= Ho, Er, Yb), space group $P6_3cm$ (C_{6v}^3) undergo different types of structural and magnetic phase transitions. The Landau theory of phase transitions is applied to study the phenomenon of phase transitions in these materials. In Landau theory, the changes in a symmetry of a crystal can be described by an order parameter, the components of which transform according to a physically irreducible representation (IR) of the high symmetry space group. A physically IR is either a real IR or the direct sum of two complex conjugate IR of high symmetry space group. An order parameter is a physical quantity such as polarization, magnetization, strain, atomic displacements etc.

A systematic method is adopted here to determine structural phase transitions in these materials. The method involves (i) selection of irreducible representation of the space group, (ii) derivation of the expression for the Landau free energy, (iii) determination of low symmetry phases, and (iv) identification of point groups and space groups for low symmetry phases. In order to work out all possible phase transitions occurring in $RMnO_3$ compounds, it is necessary to consider different IR's of the space group $P6_3cm$. The IR's at the Γ point of the hexagonal Brillouin zone are considered.

The Γ point lies at the origin of Brillouin zone and coordinates of the wave vector $\mathbf{k}$ are $(k_x, k_y, k_z) = (0, 0, 0)$. The IR's of the space group $P6_3cm$ at the Γ point are same as those of the point group C_{6v} and are denoted by A_1, A_2, B_1, B_2, E_1, E_2. The IR's A_1, A_2, B_1, B_2 are one dimensional while E_1, E_2 are two dimensional IR's. The character tables of these IR's are given in Appendix A.

3.1 Landau Free Energy for One-dimensional Order Parameters

3.1.1 Landau Free Energy for A_1

The Landau free energy is a polynomial expansion in the order parameter η. The Landau free energy for one dimensional IR A_1 to fourth order is [73]:

$$F(\eta) = \frac{\alpha}{2}\eta^2 + \frac{\beta}{3}\eta^3 + \frac{\gamma}{4}\eta^4. \tag{3.1}$$

It is invariant under all symmetry operations of the high symmetry space group $P6_3cm$ on the order parameter η.

In order to find the phase transition between the high symmetry and the low symmetry phases, it is necessary to minimize F. The equations minimizing F are:

$$\frac{\partial F}{\partial \eta} = \alpha\eta + \beta\eta^2 + \gamma\eta^3 = 0, \tag{3.2}$$

$$\frac{\partial^2 F}{\partial \eta^2} = \alpha + 2\beta\eta + 3\gamma\eta^2 \geq 0. \tag{3.3}$$

The three solutions of η are: η_I=0 and $\eta_{II} = [-\beta \pm (\beta^2 - 4\alpha\gamma)^{1/2}]/2\gamma$. Thus from the above conditions of minimization, one finds that the η_I=0 phase, called the parent phase I, is stable and corresponds to the minimum of F for $\alpha > 0$ as shown in Figure 3.1. The minimum for phase I persists for $\alpha > 0$ as shown in Figure 3.2. There exits

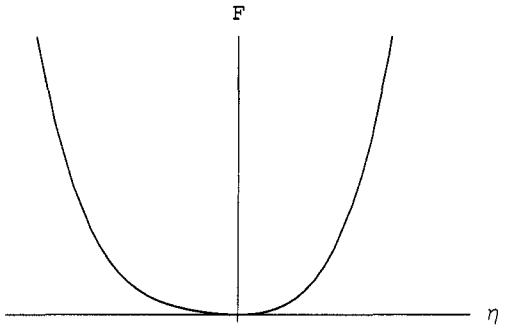

Figure 3.1: The plot of F versus η for $\alpha > 0$ shows the minimum at η=0, which is phase I.

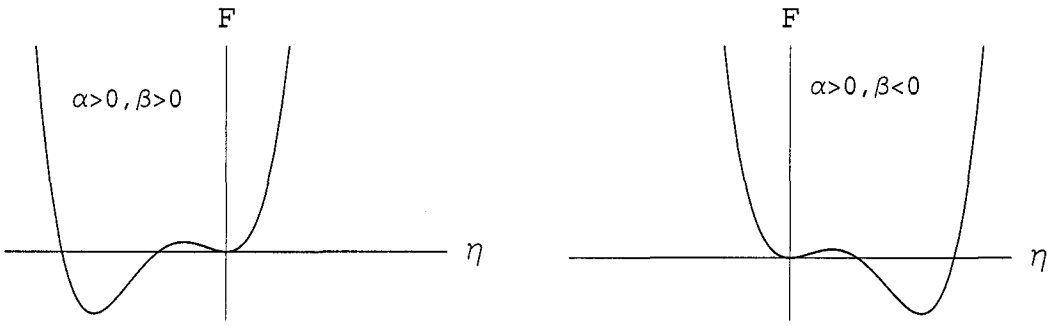

Figure 3.2: The plot of F versus η for $\alpha > 0$, $\beta > 0$ or $\beta < 0$. In this case the minimum at η=0 correspond to the metastable phase while the minima at $\eta_{II} = [-\beta \pm (\beta^2 - 4\alpha\gamma)^{1/2}]/2\gamma$ correspond to the stable phase.

two minima corresponding to two non-zero values of η_{II} i.e.,
$\eta_{II} = [-\beta \pm (\beta^2 - 4\alpha\gamma)^{1/2}]/2\gamma$, which persist for $\beta^2 \geq 4\alpha\gamma$, called limit of stability of phase II as shown in Figure 3.3.

The transition occurs for $\alpha = 2\beta^2/9\gamma$ and is obtained by equating the free energy for η_I and η_{II},i.e., $F(\eta_I) = F(\eta_{II})$. Here $\eta_{II} = [-\beta + (\beta^2 - 4\alpha\gamma)^{1/2}]/2\gamma$, because the minimum at $\eta_{II} = [-\beta + (\beta^2 - 4\alpha\gamma)^{1/2}]/2\gamma$ goes below the minimum at
$\eta_{II} = [-\beta - (\beta^2 - 4\alpha\gamma)^{1/2}]/2\gamma$ or one can say that the minimum at

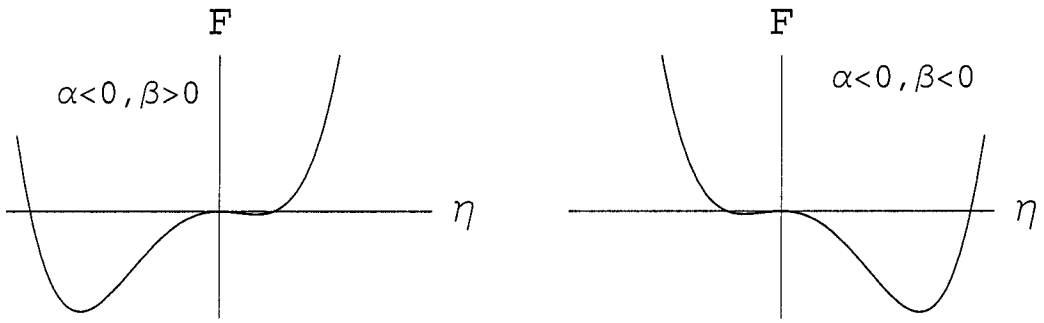

Figure 3.3: The plot of F versus η for α <0, β >0 or β <0. Here the minimum at $\eta_{II} = [-\beta + (\beta^2 - 4\alpha\gamma)^{1/2}]/2\gamma$ correspond to the stable phase while the minimum at $\eta_{II} = [-\beta - (\beta^2 - 4\alpha\gamma)^{1/2}]/2\gamma$ correspond to the metastable phase which is phase II.

$\eta_{II} = [-\beta + (\beta^2 - 4\alpha\gamma)^{1/2}]/2\gamma$ correspond to the stable phase while the minimum at $\eta_{II} = [-\beta - (\beta^2 - 4\alpha\gamma)^{1/2}]/2\gamma$ correspond to the metastable phase. This transition is of first order because $\eta_I \neq \eta_{II}$ along the transition line $\alpha = 2\beta^2/9\gamma$. The phase diagram in (α, β) plane for the free energy given in (3.1) is shown in Figure 3.4 by keeping γ positive as required for the conditions of stability.

3.1.2 Landau Free Energy for A_2, B_1 and B_2

The expression for the Landau free energy for the one dimensional IR's A_2, B_1, B_2 up to sixth order can be written as [73]:

$$F(\eta) = \frac{\alpha}{2}\eta^2 + \frac{\beta}{4}\eta^4 + \frac{\gamma}{6}\eta^6. \tag{3.4}$$

In this case the cubic term is absent from free energy because it is not invariant under all symmetry operations of space group $P6_3cm$.

In order to find out a first order and second order transition between the high symmetry and the low symmetry phases, it is necessary to minimize F. The equations

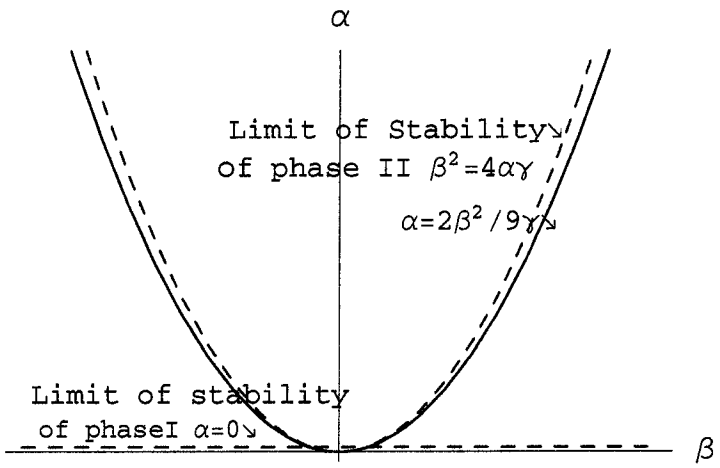

Figure 3.4: The phase diagram corresponding to the free energy $F(\eta)$ in (3.1). The blue solid line and dashed red lines are limit of stability and first order transition lines respectively.

minimizing F are:

$$\frac{\partial F}{\partial \eta} = \alpha\eta + \beta\eta^3 + \gamma\eta^5 = 0, \tag{3.5}$$

$$\frac{\partial^2 F}{\partial \eta^2} = \alpha + 3\beta\eta^2 + 5\gamma\eta^4 \geq 0. \tag{3.6}$$

The three solutions of η are: η_I=0 and $\eta_{II}^2 = [-\beta \pm (\beta^2 - 4\alpha\gamma)^{1/2}]/2\gamma$.

There is a minima in F corresponding to η_I=0 for α >0, namely the parent phase(I). The minimum for phase I persists for α >0. The phase II appears for non zero value of $\eta_{II}^2 = [-\beta \pm (\beta^2 - 4\alpha\gamma)^{1/2}]/2\gamma$ and is stable for α <0. The plot of F versus η for different values of α and β is shown in Figure 3.5 by keeping γ constant. By considering γ greater than zero, one gets the phase diagram in the (α, β) plane as shown in Figure 3.6 for the free energy given in (3.4). The line of phase transition is described by $\alpha = 3\beta^2/16\gamma$ when β <0, which is determined by equating the free energy at η_I and η_{II}, i.e., $F(\eta_I) = F(\eta_{II})$, while for β >0 the transition is along α=0. The transition for β <0 is first order, because $\eta_I \neq \eta_{II}$ along the transition line

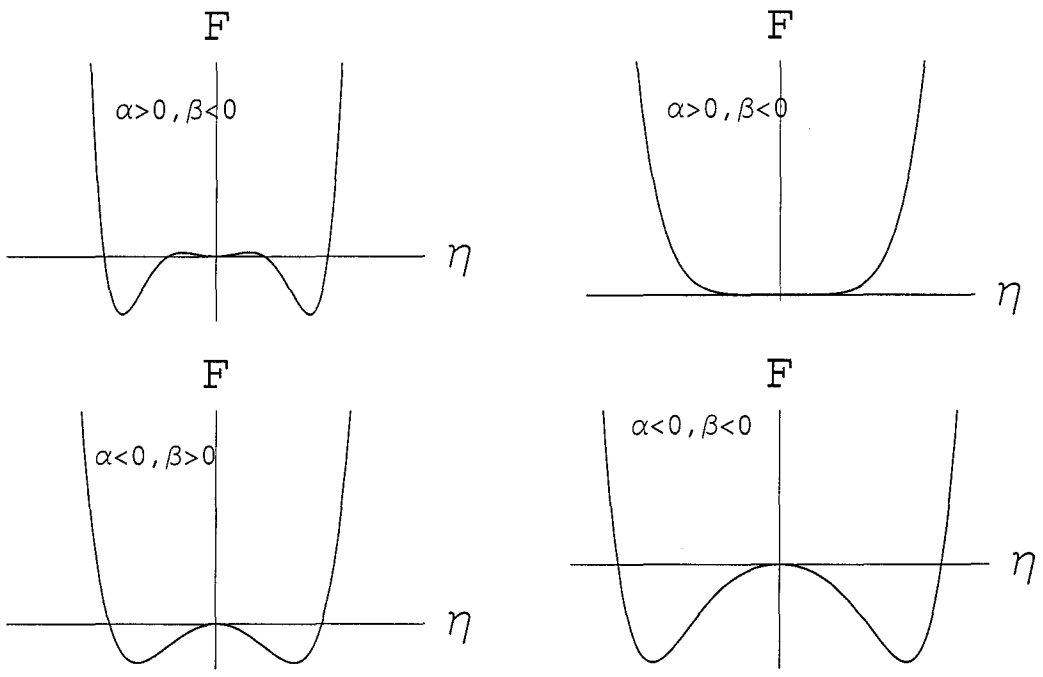

Figure 3.5: The plot of F versus η for various values of α and β.

$\alpha = 3\beta^2/16\gamma$. The transition for $\beta > 0$ is second order because $\eta_I = \eta_{II} = 0$ along the transition line. When $\beta < 0$, the minima of η_{II} persists for $\beta^2 \geq 4\alpha\gamma$.

The low symmetry phases for one dimensional order parameters at the Γ point in a crystal with $P6_3cm$ symmetry is given in the Table 3.1.

3.2 Landau Free Energy for Two-dimensional Order Parameter

3.2.1 Landau Free Energy for E_1

The two dimensional IR's E_1 and E_2 in C_{6v}^3 correspond to two component order parameters. In the case of E_1, the sixth order expansion of Landau free energy F as

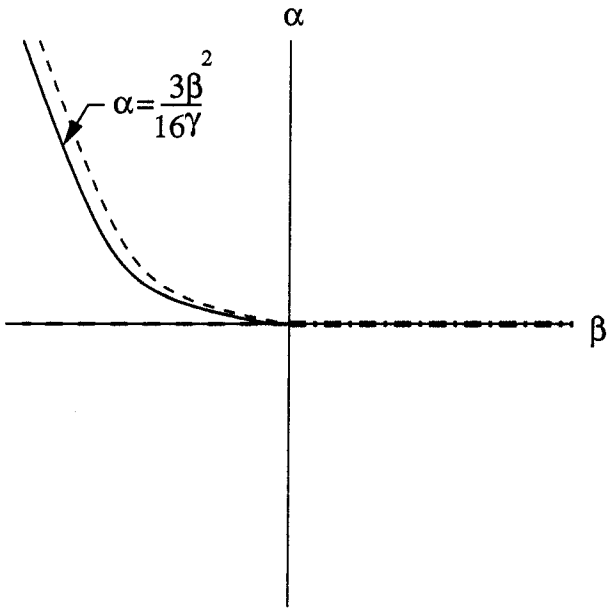

Figure 3.6: The phase diagram corresponding to the free energy $F(\eta)$ in (3.4). The solid blue line, dotted dashed green line and red dashed lines are first order, second order and limit of stability lines respectively.

Point on h-BZ	Irreducible Representation	Space Group
Γ	A_1	$P6_3cm$ (C_{6v}^3)
	A_2	$P6_3$ (C_6^6)
	B_1	$P3c1$ (C_{3v}^3)
	B_2	$P31m$ (C_{3v}^2)

Table 3.1: Low symmetry phases resulting from structural phase transitions for one-dimensional IR at the Γ point in a crystal with $P6_3cm$ symmetry.

a function of the two component order parameters η_1 and η_2 can be expressed as [73]:

$$F(\eta_1, \eta_2) = a_1(\eta_1^2 + \eta_2^2) + a_2(\eta_1^2 + \eta_2^2)^2 + a_3(\eta_1^2 + \eta_2^2)^3 + b_1(\eta_1^3 - 3\eta_1\eta_2^2)^2. \quad (3.7)$$

Using cylindrical coordinates wit $\eta_1 = \rho\cos\theta$ and $\eta_2 = \rho\sin\theta$, $F(\eta_1, \eta_2)$ becomes:

$$F(\rho, \theta) = a_1\rho^2 + a_2\rho^4 + a_3\rho^6 + b_1\rho^6\cos^2 3\theta. \quad (3.8)$$

The equations minimizing F are:

$$\frac{\partial F}{\partial \rho} = 2a_1\rho + 4a_2\rho^3 + 6a_3\rho^6 + 6b_1\rho^5\cos^2 3\theta = 0, \quad (3.9)$$

$$\frac{\partial F}{\partial \theta} = -6b_1\rho^6\cos 3\theta \sin 3\theta = 0. \quad (3.10)$$

From (3.9) and (3.10), one can see that in addition to the parent phase I (ρ=0, η_1=0, η_2=0) there exist two types of solutions corresponding to different classes of low symmetry phases. These are determined by the equation $\cos 3\theta \sin 3\theta$=0. For $\cos 3\theta$=0, $\sin 3\theta = \pm 1$, so $F(\rho, \theta)$ becomes

$$F(\rho, \theta) = a_1\rho^2 + a_2\rho^4 + a_3\rho^6. \quad (3.11)$$

For $\sin 3\theta$=0, $\cos 3\theta = \pm 1$, so $F(\rho, \theta)$ becomes

$$F(\rho, \theta) = a_1\rho^2 + a_2\rho^4 + a_3\rho^6 + b_1\rho^6. \quad (3.12)$$

One gets, from (3.10) and (3.11) that the minima of F depends on the sign of b_1 i.e., $\sin 3\theta$=0 solutions correspond to the minima in F if b_1 <0, or $\cos 3\theta$=0 solutions is minima if b_1 >0.

Thus the two low symmetry phases are denoted by phase II for $\cos 3\theta = \pm 1$ and phase III for $\sin 3\theta = \pm 1$ correspond to the equilibrium values (η,0) and (0,η) re-

spectively and equivalent domains obtained by applying the operations of C_{6v}^3. The possible symmetry of phase II and phase III is Pm(C^1s) and Pc(C^2s) respectively.

3.2.2 Landau Free Energy for E_2

The Landau expansion for E_2 is different from E_1 because of symmetry operation C_2, which leaves the third order term invariant for E_2 but not for E_1. So finally, the fourth order Landau expansion F for E_2 is [73]:

$$F(\eta_1, \eta_2) = a_1(\eta_1^2 + \eta_2^2) + b_1(\eta_1^3 - 3\eta_1\eta_2^2) + a_2(\eta_1^2 + \eta_2^2)^2. \quad (3.13)$$

In terms of cylindrical coordinates equation (3.11) becomes

$$F(\rho, \theta) = a_1\rho^2 + b_1\rho^3 cos3\theta + a_2\rho^4 \quad (3.14)$$

The equations minimizing F are:

$$\frac{\partial F}{\partial \rho} = 2a_1\rho + 3b_1\rho^2 cos3\theta + 4a_2\rho^3 = 0, \quad (3.15)$$

$$\frac{\partial F}{\partial \theta} = -3b_1\rho^3 sin3\theta = 0. \quad (3.16)$$

From (3.16), $\sin 3\theta$=0 for $\cos 3\theta = \pm 1$. Therefore (3.15) and (3.16)give, in addition to the parent phase I (ρ=0, η_1=0, η_2=0), the two low symmetry phases of identical symmetry. These phases are denoted by phase II for $\cos 3\theta$=1 and phase III for $\cos 3\theta$=-1 corresponding to the equilibrium values (η,0) and (-η,0) respectively and equivalent domains obtained by applying operations of C_{6v}^3. The symmetry group associated with phase II and phase III is $Cmc2_1$ (C_{2v}^{12}).

C_{6v}	E	$2C_6$	$2C_3$	C_2	$3\sigma_v$	$3\sigma_d$	t_1	t_2	t_3
M_1	3	0	0	3	1	1	-1	-1	3
M_2	3	0	0	3	-1	-1	-1	-1	3
M_3	3	0	0	-3	1	-1	-1	-1	3
M_4	3	0	0	-3	-1	1	-1	-1	3

Table 3.2: The irreducible representations of the space group $P6_3cm$ at the M-point on the hexagonal Brillouin zone.

3.3 Landau Free Energy at the M-Point

A theoretical analysis is presented here for the structural phase transitions at the M-point of the hexagonal Brillouin zone as an example of a non-zero k-vector. M-point is the center of the rectangular face and its symmetry group is D_{2h}. The wave vector $\mathbf{k}$ at the M-point is $(1/2)\mathbf{b}_2$, where $\mathbf{b}_2=\frac{2\pi}{a}(\frac{2}{\sqrt{3}}, 0, 0)$ is a reciprocal lattice vector of the hexagonal system. The IR of the space group $P6_3cm$ at the M-point are calculated by specifying the IR of the little group. The little group in this case is C_{2v} which has four one dimensional IR's. The dimension of the IR of a space group ($P6_3cm$) at the M-point is a product of dimension of IR's in a little group C_{2v} and number of arms in k*. k* is generated by applying all symmetry elements of point group C_{6v}^3 on wave vector at the M-point. Some of the symmetry elements of point group C_{6v}^3 will leave the wave vector unchanged, therefore k* has the following three arms: $(0\ \frac{1}{2}\ 0)$, $(\frac{1}{2}\ \frac{1}{2}\ 0)$, $(\frac{1}{2}\ 0\ 0)$. Thus there are four three-dimensional IR's, namely M_1, M_2, M_3 and M_4 at the M-point of the hexagonal Brillouin zone. The characters of these IR's along with the translations are given in the Table 3.2. The matrices of the representations M_1, M_2, M_3 and M_4 along with translations t_1, t_1 and t_3 are given in Appendix A.

The fourth-order Landau expansion for the M point is written as [64]:

$$F(\eta_1,\eta_2,\eta_3) = \frac{\alpha}{2}(\eta_1^2+\eta_2^2+\eta_3^2)+\frac{\beta_1}{4}(\eta_1^4+\eta_2^4+\eta_3^4)+\frac{\beta_2}{2}(\eta_1^2\eta_2^2+\eta_2^2\eta_3^2+\eta_1^2\eta_3^2). \tag{3.17}$$

From minimization of F with respect to η_1, η_2, η_3, one finds in addition to the parent phase I (η_1=0, η_2=0, η_3=0),three different low symmetry phases. These phases are denoted by phase II, phase III and phase IV and correspond to the equilibrium values (η, η, η), (η, η, 0), (η, 0, 0) respectively, and equivalent domains found by applying symmetry operations of C_{6v}^3. The Landau free energy at the M point of the hexagonal BZ is equivalent to the free energy for the three-dimensional representations of O_h. Therefore, results can be obtained by considering the phase diagram of O_h.

The possible structural phase transitions of Landau type for three dimensional IR at the M-point in a crystal with $P6_3cm$ symmetry is given in the Table 3.3.

3.4 Summary

The structural phase transitions occurring at the Γ point and at the M-point of the hexagonal Brillouin zone are found by using Landau theory of phase transitions. Also the Landau free energy corresponding to one-dimensional irreducible representation A_1, A_2, B_1, B_2, E_1 and E_2 at the Γ and three-dimensional representation M_1, M_2, M_3 and M_4 at the M-point has been determined. The low symmetry phases corresponding to A_1, A_2, B_1, B_2 are $P6_3cm$ (C_{6v}^3), $P6_3$ (C_6^6), P3c1 (C_{3v}^3) and P31m (C_{3v}^2). The low symmetry phases for E_1 are Pm(C^1s) and Pc(C^2s), while for E_2 the two low symmetry phases correspond to same space group $Cmc2_1$ (C_{2v}^{12}).

For M_1 the low symmetry phases are $P6_3cm$ (C_{6v}^3), $Cmc2_1$ (C_{2v}^{12}) and $Pmc2_1$ (C_{2v}^1). For M_2 the low symmetry phases are $P6_3$ (C_6^6), $Cmc2_1$ (C_{2v}^3) and $Pmn2_1$ (C_{2v}^7). For M_3 the low symmetry phases are P3c1 (C_{3v}^3), Cc (C_s^4)and Pc (C_s^2). Finally, for M_4

Point on h-BZ	Irreducible Representation	Order Parameter Space	Space Group
M	M_1	$\eta\ \eta\ \eta$	$P6_3cm$ (C_{6v}^3)
		$\eta\ \eta\ 0$	$Cmc2_1$ (C_{2v}^{12})
		$\eta\ 0\ 0$	$Pmc2_1$ (C_{2v}^1)
	M_2	$\eta\ \eta\ \eta$	$P6_3$ (C_6^6)
		$\eta\ \eta\ 0$	$Cmc2_1$ (C_{2v}^3)
		$\eta\ 0\ 0$	$Pmn2_1$ (C_{2v}^7)
	M_3	$\eta\ \eta\ \eta$	P3c1 (C_{3v}^3)
		$\eta\ \eta\ 0$	Cc (C_s^4)
		$\eta\ 0\ 0$	Pc (C_s^2)
	M_4	$\eta\ \eta\ \eta$	P31m (C_{3v}^2)
		$\eta\ \eta\ 0$	Cm (C_s^3)
		$\eta\ 0\ 0$	Pm (C_s^1)

Table 3.3: Low symmetry phases resulting from the structural phase transitions for IR at the M-point in a crystal with $P6_3cm$ symmetry.

the low symmetry phases are P31m (C_{3v}^2), Cm (C_s^3)and Pm (C_s^1).

Chapter 4

Final Remarks

4.1 Conclusions

Different types of structural and magnetic phase transitions take place in hexagonal perovskites $RMnO_3$ for R=Ho, Er, Yb. The Landau theory of phase transitions is a useful tool to study the structural and magnetic changes in these materials, in which a symmetry breaking order parameter is required that transforms like irreducible representations of the high symmetry space group. The possible symmetry changes that can take place in a crystal with $P6_3cm$ symmetry at the Γ point are analyzed. The structural phases resulting from one component order parameters A_1, A_2, B_1, B_2 have symmetry $P6_3cm$ (C_{6v}^3), $P6_3$ (C_6^6), P3c1 (C_{3v}^3) and P31m (C_{3v}^2) respectively. The structural phases, which appear in case of the two component order parameter E_1 have two low symmetry phases Pm (C_s^1), Pc (C_s^2) corresponding to the equilibrium values $(\eta,0)$, $(0,\eta)$, and for E_2 the two low symmetry phases correspond to the same symmetry group $Cmc2_1$ (C_{2v}^{12}) but with opposite values of equilibrium order parameter i.e., $(\eta,0)$, $(-\eta,0)$.

The phase transitions occurring at the M-point of hexagonal Brillouin zone are

investigated for a crystal with $P6_3cm$ symmetry. The space group representations appearing at the M-point are three-dimensional denoted by M_1, M_2, M_3 and M_4. The low symmetry phases as a result of structural phase transitions at M_1 has symmetry $P6_3cm$ (C_{6v}^3), $Cmc2_1$ (C_{2v}^{12}) and $Pmc2_1$ (C_{2v}^1) corresponding to the equilibrium values (η, η, η), (η, η, 0) and (η, 0, 0). The low symmetry phases appearing at M_2 has symmetry $P6_3$ (C_6^6), $Cmc2_1$ (C_{2v}^{12}) and $Pmn2_1$ (C_{2v}^7) corresponding to the equilibrium values (η, η, η), (η, η, 0) and (η, 0, 0). For M_3, the low symmetry phase corresponding to equilibrium values (η, η, η) is P3c1 (C_{3v}^3), while (η, η, 0) and (η, 0, 0) are associated with the symmetries Cc (C_s^4) and Pc (C_s^2). For M_4, the low symmetry phase corresponding to equilibrium values (η, η, η) is P31m (C_{3v}^2), while (η, η, 0) and (η, 0, 0) are associated with the symmetries Cm (C_s^3) and Pm (C_s^1).

4.2 Suggestions for Further Work

The magnetic transitions in $RMnO_3$ compounds are due to antiferromagnetic ordering of Mn^{3+} sublattices and in some compounds due to antiferromagnetic/ferromagnetic ordering R^{3+} sublattices. The magnetic symmetries of $RMnO_3$ compounds because of Mn^{3+} sublattices are $P6_3cm$, $P6_3\underline{cm}$, $P\underline{6}_3c\underline{m}$ and $P\underline{6}_3\underline{c}m$ corresponding to one component order parameter A_1, A_2, B_1, B_2 respectively. The rare earth ions develop magnetic moment at very low temperature $\approx$ 5K but their magnetic structures are still under investigation. However, it is suspected that the magnetic symmetry changes from $P6_3cm$ to Pc for $HoMnO_3$ and $P\underline{c}$ for $ErMnO_3$, $YbMnO_3$ [19]. The irreducible representation E_1 at the Γ point or M_3 representation at the M-point of the hexagonal Brillouin zone are proposed to be related to this symmetry for $HoMnO_3$.

Appendix A

Hexagonal Crystal System

The hexagonal crystal system has four axes of symmetry. Three of them are of equal lengths set at 120^o to one another, and the fourth one is perpendicular to the plane of first three. These axes are denoted by a_1, a_2, a_3 and C respectively and are shown in Figure A.1.

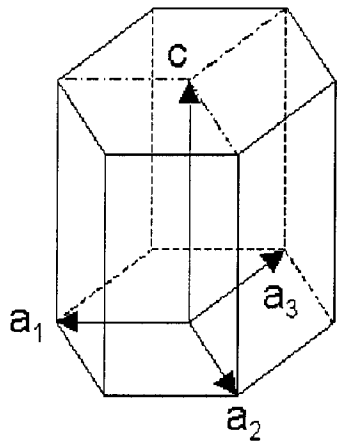

Figure A.1: Indexing of Hexagonal Lattice.

The volume of the hexagonal unit cell is $\frac{\sqrt{3}}{2}a^2c$. The lattice vectors are:

$\mathbf{g}_1$=(0, -a, 0); $\mathbf{g}_2$=$\frac{1}{2}$(a$\sqrt{3}$, a, 0); $\mathbf{g}_3$=(0, 0, c)

The reciprocal lattice vectors are:

$\mathbf{b}_1=\frac{2\pi}{a}(\frac{1}{\sqrt{3}}, -1, 0)$; $\mathbf{b}_2=\frac{2\pi}{a}(\frac{2}{\sqrt{3}}, 0, 0)$; $\mathbf{b}_3=\frac{2\pi}{c}(0, 0, 1)$

The Brillouin zone (BZ) of the hexagonal lattice is shown in Figure A.2 and has volume= $\frac{16\pi^3}{\sqrt{3}a^2c}$. The points and lines of symmetry of the hexagonal BZ and their coordinates with respect to $\mathbf{b}_1$, $\mathbf{b}_2$ and $\mathbf{b}_3$ are listed in a Table A.1. For example, P is a point on the line KH and its $\mathbf{k}$ vector is $(-\frac{1}{3}\mathbf{b}_1+\frac{2}{3}\mathbf{b}_2+\alpha\mathbf{b}_3)=(-\frac{1}{3}\frac{2}{3}\alpha)$, $0< \alpha < \frac{1}{2}$.

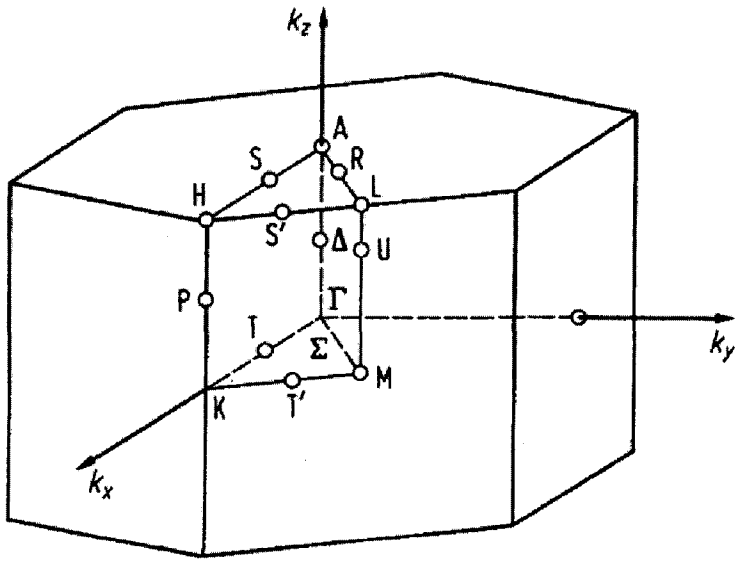

Figure A.2: Brillouin zone of the hexagonal lattice [53].

A.1 Space Group $P6_3cm(C_{6v}^3)$

The space group $P6_3cm$ [#185,(C_{6v}^3)] belongs to the class of hexagonal crystal system and has twelve symmetry elements. These symmetry elements consist of the identity (E), rotations by angles of $\frac{1}{3}n\pi$ radians (C_6, C_3, C_2, C_3^2, and C_6^5 for n=1, 2, 3, 4, 5 respectively), three mirror planes ($3\sigma_v$) that pass through opposite faces of the hexagon, and three mirror planes ($3\sigma_d$) that pass through opposite vertices of the

Bravais Lattice	Point/Line of Symmetry	Coordinates
Hexagonal P, Γ_h	Γ	(0 0 0)
	M	(0 $\frac{1}{2}$ 0)
	A	(0 0 $\frac{1}{2}$ 0)
	L	(0 $\frac{1}{2}$ $\frac{1}{2}$)
	K	(-$\frac{1}{3}$ $\frac{2}{3}$ 0)
	H	(-$\frac{1}{3}$ $\frac{2}{3}$ $\frac{1}{2}$)
	$\Delta(\Gamma A)$	(0 0 α)
	U(ML)	(0 $\frac{1}{2}$ α)
	P(KH)	(-$\frac{1}{3}$ $\frac{2}{3}$ α)
	T(ΓK)	(-α, 2α, 0)
	S(AH)	(-α, 2α, $\frac{1}{2}$)
	T'(MK)	(-2α, $\frac{1}{2}$+α, 0)
	S'(LH)	(-2α, $\frac{1}{2}$+α, $\frac{1}{2}$)
	$\Sigma(\Gamma M)$	(0 α 0)
	R(AL)	(0 α $\frac{1}{2}$)

Table A.1: List of points of the hexagonal Brillouin zone [53].

1	E	x, y, z	7	σ_{v1}	$-x+y, y, z+\frac{1}{2}$
2	C_3	$-y, x-y, z$	8	σ_{v2}	$x, x-y, z+\frac{1}{2}$
3	C_3^2	$-x+y, -x, z$	9	σ_{v3}	$-y, -x, z+\frac{1}{2}$
4	C_2	$-x, -y, z+\frac{1}{2}$	10	σ_{d1}	$x-y, -y, z$
5	C_6	$x-y, x, z+\frac{1}{2}$	11	σ_{d2}	$-x, -x+y, z$
6	C_6^5	$y, -x+y, z+\frac{1}{2}$	12	σ_{d3}	y, x, z

Table A.2: Positions of symmetry elements of space group $P6_3cm$ [54].

hexagon. The generators of the group are E, C_3, C_2 and σ_{v3}. It is a nonsymmorphic space group and involves glide reflections and screw rotations. In this case three mirror planes ($3\sigma_v$) are glide planes. The general positions of all twelve symmetry elements are given in Table A.2.

The stereographic projection of C_{6v}^3 is shown in Figure A.3..

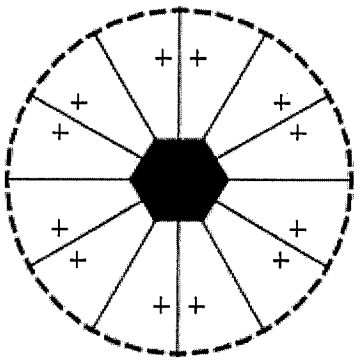

Figure A.3: The stereographic projection of C_{6v}^3 [51].

A.1.1 Character Table of C_{6v}^3

The Γ point lies at the origin of the hexagonal BZ with wave vector **k**=(0, 0, 0). The character table of irreducible representations and their products at the Γ-point for the point group C_{6v}^3 is shown in the Table A.3 and Table A.4 respectively.

C_{6v}^3	E	$2C_6$	$2C_3$	C_2	$3\sigma_v$	$3\sigma_d$	Linear Functions	Quadratic Functions
A_1	1	1	1	1	1	1	z	x^2+y^2,z^2
A_2	1	1	1	1	-1	-1	R_z	–
B_1	1	-1	1	-1	1	-1	–	–
B_2	1	-1	1	-1	-1	1	–	–
E_1	2	1	-1	-2	0	0	$(x,y)(R_x,R_y)$	(xz,yz)
E_2	2	-1	-1	2	0	0	–	(x^2-y^2,xy)

Table A.3: Character table of the Γ point representations of C_{6v}^3 [51].

C_{6v}^3	A_1	A_2	B_1	B_2	E_1	E_2
A_1	A_1	A_2	B_1	B_2	E_1	E_2
A_2	A_2	A_1	B_2	B_1	E_1	E_2
B_1	B_1	B_2	A_1	A_2	E_2	E_1
B_2	B_2	B_1	A_2	A_1	E_2	E_1
E_1	E_1	E_1	E_2	E_2	$A_1+A_2+E_2$	$B_1+B_2+E_1$
E_2	E_2	E_2	E_1	E_1	$B_1+B_2+E_1$	$A_1+A_2+E_2$

Table A.4: Irreducible representation products of C_{6v}^3.

A.1.2 Matrices at the Γ-Point of the Hexagonal Brillouin Zone

An explicit form for matrices of the irreducible representations E_1 and E_2 of the point group C_{6v}^3 are as follows:

Matrices of E_1

$$E = \begin{pmatrix} 1 & 0 \\ 0 & 1 \end{pmatrix}, \quad C_3 = \begin{pmatrix} -\frac{1}{2} & \frac{\sqrt{3}}{2} \\ -\frac{\sqrt{3}}{2} & -\frac{1}{2} \end{pmatrix}, \quad C_3^2 = \begin{pmatrix} -\frac{1}{2} & -\frac{\sqrt{3}}{2} \\ \frac{\sqrt{3}}{2} & -\frac{1}{2} \end{pmatrix}, \quad C_2 = \begin{pmatrix} -1 & 0 \\ 0 & -1 \end{pmatrix}$$

$$C_6 = \begin{pmatrix} \frac{1}{2} & \frac{\sqrt{3}}{2} \\ -\frac{\sqrt{3}}{2} & \frac{1}{2} \end{pmatrix}, \quad C_6^5 = \begin{pmatrix} \frac{1}{2} & -\frac{\sqrt{3}}{2} \\ \frac{\sqrt{3}}{2} & \frac{1}{2} \end{pmatrix}, \quad \sigma_{v1} = \begin{pmatrix} -1 & 0 \\ 0 & 1 \end{pmatrix}, \quad \sigma_{v2} = \begin{pmatrix} \frac{1}{2} & \frac{\sqrt{3}}{2} \\ \frac{\sqrt{3}}{2} & -\frac{1}{2} \end{pmatrix},$$

$$\sigma_{v3} = \begin{pmatrix} \frac{1}{2} & -\frac{\sqrt{3}}{2} \\ -\frac{\sqrt{3}}{2} & -\frac{1}{2} \end{pmatrix}, \quad \sigma_{d1} = \begin{pmatrix} 1 & 0 \\ 0 & -1 \end{pmatrix}, \quad \sigma_{d2} = \begin{pmatrix} -\frac{1}{2} & -\frac{\sqrt{3}}{2} \\ -\frac{\sqrt{3}}{2} & \frac{1}{2} \end{pmatrix}, \quad \sigma_{d3} = \begin{pmatrix} -\frac{1}{2} & \frac{\sqrt{3}}{2} \\ \frac{\sqrt{3}}{2} & \frac{1}{2} \end{pmatrix} \tag{A.1}$$

Matrices of E_2

$$E = \begin{pmatrix} 1 & 0 \\ 0 & 1 \end{pmatrix}, \quad C_3 = \begin{pmatrix} -\frac{1}{2} & -\frac{\sqrt{3}}{2} \\ \frac{\sqrt{3}}{2} & -\frac{1}{2} \end{pmatrix}, \quad C_3^2 = \begin{pmatrix} -\frac{1}{2} & \frac{\sqrt{3}}{2} \\ -\frac{\sqrt{3}}{2} & -\frac{1}{2} \end{pmatrix}, \quad C_2 = \begin{pmatrix} 1 & 0 \\ 0 & 1 \end{pmatrix}$$

$$C_6 = \begin{pmatrix} -\frac{1}{2} & \frac{\sqrt{3}}{2} \\ -\frac{\sqrt{3}}{2} & -\frac{1}{2} \end{pmatrix}, \quad C_6^5 = \begin{pmatrix} -\frac{1}{2} & -\frac{\sqrt{3}}{2} \\ \frac{\sqrt{3}}{2} & -\frac{1}{2} \end{pmatrix}, \quad \sigma_{v1} = \begin{pmatrix} 1 & 0 \\ 0 & -1 \end{pmatrix}, \quad \sigma_{v2} = \begin{pmatrix} -\frac{1}{2} & \frac{\sqrt{3}}{2} \\ \frac{\sqrt{3}}{2} & \frac{1}{2} \end{pmatrix},$$

$$\sigma_{v3} = \begin{pmatrix} -\frac{1}{2} & -\frac{\sqrt{3}}{2} \\ -\frac{\sqrt{3}}{2} & \frac{1}{2} \end{pmatrix}, \quad \sigma_{d1} = \begin{pmatrix} 1 & 0 \\ 0 & -1 \end{pmatrix}, \quad \sigma_{d2} = \begin{pmatrix} -\frac{1}{2} & \frac{\sqrt{3}}{2} \\ \frac{\sqrt{3}}{2} & \frac{1}{2} \end{pmatrix}, \quad \sigma_{d3} = \begin{pmatrix} -\frac{1}{2} & -\frac{\sqrt{3}}{2} \\ -\frac{\sqrt{3}}{2} & \frac{1}{2} \end{pmatrix} \tag{A.2}$$

A.1.3 Matrices at the M-Point of the Hexagonal Brillouin Zone

The M point is the center of the rectangular face with wave vector $\mathbf{k}=(0\ \frac{1}{2}\ 0)$ as shown in the Brillouin zone of the hexagonal lattice in Fig A.2. There are four three-dimensional space group representations at the M-point, namely M_1, M_2, M_3, M_4. The matrices of these four three-dimensional representations are as follows:

Matrices of M_1

$$E=\begin{pmatrix}1&0&0\\0&1&0\\0&0&1\end{pmatrix},\quad C_3=\begin{pmatrix}0&0&1\\1&0&0\\0&1&0\end{pmatrix},\quad C_3^2=\begin{pmatrix}0&1&0\\0&0&1\\1&0&0\end{pmatrix},\quad C_2=\begin{pmatrix}1&0&0\\0&1&0\\0&0&1\end{pmatrix}$$

$$C_6=\begin{pmatrix}0&1&0\\0&0&1\\1&0&0\end{pmatrix},\quad C_6^5=\begin{pmatrix}0&0&1\\1&0&0\\0&1&0\end{pmatrix},\quad \sigma_{v1}=\begin{pmatrix}0&1&0\\1&0&0\\0&0&1\end{pmatrix},\quad \sigma_{v2}=\begin{pmatrix}1&0&0\\0&0&1\\0&1&0\end{pmatrix},$$

$$\sigma_{v3}=\begin{pmatrix}0&0&1\\0&1&0\\1&0&0\end{pmatrix},\quad \sigma_{d1}=\begin{pmatrix}0&1&0\\1&0&0\\0&0&1\end{pmatrix},\quad \sigma_{d2}=\begin{pmatrix}1&0&0\\0&0&1\\0&1&0\end{pmatrix},\quad \sigma_{d3}=\begin{pmatrix}0&0&1\\0&1&0\\1&0&0\end{pmatrix} \tag{A.3}$$

Matrices of M_2

$$E=\begin{pmatrix}1&0&0\\0&1&0\\0&0&1\end{pmatrix},\quad C_3=\begin{pmatrix}0&0&1\\1&0&0\\0&1&0\end{pmatrix},\quad C_3^2=\begin{pmatrix}0&1&0\\0&0&1\\1&0&0\end{pmatrix}$$

$$C_2=\begin{pmatrix}1&0&0\\0&1&0\\0&0&1\end{pmatrix},\quad C_6=\begin{pmatrix}0&1&0\\0&0&1\\1&0&0\end{pmatrix},\quad C_6^5=\begin{pmatrix}0&0&1\\1&0&0\\0&1&0\end{pmatrix},$$

$$\sigma_{v1}=\begin{pmatrix}0&-1&0\\-1&0&0\\0&0&-1\end{pmatrix},\quad \sigma_{v2}=\begin{pmatrix}-1&0&0\\0&0&-1\\0&-1&0\end{pmatrix},\quad \sigma_{v3}=\begin{pmatrix}0&0&-1\\0&-1&0\\-1&0&0\end{pmatrix},\tag{A.4}$$

$$\sigma_{d1}=\begin{pmatrix}0&-1&0\\-1&0&0\\0&0&-1\end{pmatrix},\quad \sigma_{d2}=\begin{pmatrix}-1&0&0\\0&0&-1\\0&-1&0\end{pmatrix},\quad \sigma_{d3}=\begin{pmatrix}0&0&-1\\0&-1&0\\-1&0&0\end{pmatrix}$$

Matrices of M_3

$$E=\begin{pmatrix}1&0&0\\0&1&0\\0&0&1\end{pmatrix},\quad C_3=\begin{pmatrix}0&0&1\\1&0&0\\0&1&0\end{pmatrix},\quad C_3^2=\begin{pmatrix}0&1&0\\0&0&1\\1&0&0\end{pmatrix}$$

$$C_2=\begin{pmatrix}-1&0&0\\0&-1&0\\0&0&-1\end{pmatrix},\quad C_6=\begin{pmatrix}0&-1&0\\0&0&-1\\-1&0&0\end{pmatrix},\quad C_6^5=\begin{pmatrix}0&0&-1\\-1&0&0\\0&-1&0\end{pmatrix},$$

$$\sigma_{v1}=\begin{pmatrix}0&1&0\\1&0&0\\0&0&1\end{pmatrix},\quad \sigma_{v2}=\begin{pmatrix}1&0&0\\0&0&1\\0&1&0\end{pmatrix},\quad \sigma_{v3}=\begin{pmatrix}0&0&1\\0&1&0\\1&0&0\end{pmatrix}\tag{A.5}$$

$$\sigma_{d1}=\begin{pmatrix}0&-1&0\\-1&0&0\\0&0&-1\end{pmatrix},\quad \sigma_{d2}=\begin{pmatrix}-1&0&0\\0&0&-1\\0&-1&0\end{pmatrix},\quad \sigma_{d3}=\begin{pmatrix}0&0&-1\\0&-1&0\\-1&0&0\end{pmatrix}$$

Matrices of M_4

$$E = \begin{pmatrix} 1 & 0 & 0 \\ 0 & 1 & 0 \\ 0 & 0 & 1 \end{pmatrix}, \quad C_3 = \begin{pmatrix} 0 & 0 & 1 \\ 1 & 0 & 0 \\ 0 & 1 & 0 \end{pmatrix}, \quad C_3^2 = \begin{pmatrix} 0 & 1 & 0 \\ 0 & 0 & 1 \\ 1 & 0 & 0 \end{pmatrix}$$

$$C_2 = \begin{pmatrix} -1 & 0 & 0 \\ 0 & -1 & 0 \\ 0 & 0 & -1 \end{pmatrix}, \quad C_6 = \begin{pmatrix} 0 & -1 & 0 \\ 0 & 0 & -1 \\ -1 & 0 & 0 \end{pmatrix}, \quad C_6^5 = \begin{pmatrix} 0 & 0 & -1 \\ -1 & 0 & 0 \\ 0 & -1 & 0 \end{pmatrix},$$

$$\sigma_{v1} = \begin{pmatrix} 0 & -1 & 0 \\ -1 & 0 & 0 \\ 0 & 0 & -1 \end{pmatrix}, \quad \sigma_{v2} = \begin{pmatrix} -1 & 0 & 0 \\ 0 & 0 & -1 \\ 0 & -1 & 0 \end{pmatrix}, \quad \sigma_{v3} = \begin{pmatrix} 0 & 0 & -1 \\ 0 & -1 & 0 \\ -1 & 0 & 0 \end{pmatrix},$$

$$\sigma_{d1} = \begin{pmatrix} 0 & 1 & 0 \\ 1 & 0 & 0 \\ 0 & 0 & 1 \end{pmatrix}, \quad \sigma_{d2} = \begin{pmatrix} 1 & 0 & 0 \\ 0 & 0 & 1 \\ 0 & 1 & 0 \end{pmatrix}, \quad \sigma_{d3} = \begin{pmatrix} 0 & 0 & 1 \\ 0 & 1 & 0 \\ 1 & 0 & 0 \end{pmatrix} \tag{A.6}$$

A.1.4 Translations at the M-Point of the Hexagonal Brillouin Zone

The matrices of the translations t_1, t_2 and t_3 can be calculated by considering k* at M-point. The k* has three arms denoted by k_1=(0 $\frac{1}{2}$ 0), k_2=($\frac{1}{2}$ $\frac{1}{2}$ 0) and k_3=($\frac{1}{2}$ 0 0). A method is described below to determine the matrices of the translations.

Matrices of t_1, t_2 and t_3

Let

$$t_1 = \begin{pmatrix} e^{ik_1.a_1} & 0 & 0 \\ 0 & e^{ik_2.a_1} & 0 \\ 0 & 0 & e^{ik_3.a_1} \end{pmatrix} \tag{A.7}$$

Here $k_1=\frac{1}{2}b_2$; $k_2=\frac{1}{2}(b_1+b_2)$; $k_3=\frac{1}{2}b_1$.

Also

$b_2.a_1=0$, $(b_1+b_2).a_1=-2\pi$, $b_1.a_1=-2\pi$

Thus

$$t_1 = \begin{pmatrix} 1 & 0 & 0 \\ 0 & -1 & 0 \\ 0 & 0 & -1 \end{pmatrix} \tag{A.8}$$

Similarly, the matrices of t_2 and t_3 are:

$$t_2 = \begin{pmatrix} -1 & 0 & 0 \\ 0 & -1 & 0 \\ 0 & 0 & 1 \end{pmatrix}, \quad t_3 = \begin{pmatrix} 1 & 0 & 0 \\ 0 & 1 & 0 \\ 0 & 0 & 1 \end{pmatrix} \tag{A.9}$$

A.2 Space Group $P6_3/mmc$ (D^4_{6h})

The space group $P6_3/mmc$[#194,(D^4_{6h}] is a non symmorphic group having twenty four symmetry elements, namely E, $2C_6$, $2C_3$, C_2, $3C'_2$, $3C'_2$, ι, $2S_3$, $2S_6$, σ_h, $3\sigma_d$, $3\sigma_v$. The general positions of these twenty four symmetry elements are given in Table A.5.

The character table of irreducible representations at the Γ point for the point group D^4_{6h} is shown in the Table A.6.

1	E	x, y, z	13	ι	$-x, -y, -z$
2	C_3	$-y, x-y, z$	14	S_3^+	$-y, x-y, -z$
3	C_3^2	$-x+y, -x, z$	15	S_3^-	$y, -x+y, -z$
4	C_2	$-x, -y, z+\frac{1}{2}$	16	S_6^+	$x-y, x, -z$
5	C_6	$x-y, x, z+\frac{1}{2}$	17	S_6^-	$y, -x+y, -z$
6	C_6^5	$y, -x+y, z+\frac{1}{2}$	18	σ_h	$y, x, -z$
7	C'_{21}	$-x+y, y, -z$	19	σ_{v1}	$-x+y, y, z+\frac{1}{2}$
8	C'_{22}	$x, x-y, -z$	20	σ_{v2}	$x, x-y, z+\frac{1}{2}$
9	C'_{23}	$-y, -x, -z$	21	σ_{v3}	$-y, -x, z+\frac{1}{2}$
10	C''_{21}	$x-y, -y, -z$	22	σ_{d1}	$x-y, -y, z$
11	C''_{22}	$-x, -x+y, -z$	23	σ_{d2}	$-x, -x+y, z$
12	C''_{23}	$y, x, -z$	24	σ_{d3}	y, x, z

Table A.5: Positions of symmetry elements of space group $P6_3/mmc$ [54].

D_{6h}^4	E	$2C_6$	$2C_3$	C_2	$3C_2'$	$3C_2''$	ι	$2S_3$	$2S_6$	σ_h	$3\sigma_d$	$3\sigma_v$	–	–
A_{1g}	1	1	1	1	1	1	1	1	1	1	1	1	–	x^2+y^2,z^2
A_{2g}	1	1	1	1	-1	-1	1	1	1	1	-1	-1	R_z	–
B_{1g}	1	-1	1	-1	1	-1	1	-1	1	-1	1	-1	–	–
B_{2g}	1	-1	1	-1	-1	1	1	-1	1	-1	-1	1	–	–
E_{1g}	2	1	-1	-2	0	0	2	1	-1	-2	0	0	(R_x,R_y)	(xz,yz)
E_{2g}	2	-1	-1	2	0	0	2	-1	-1	2	0	0	–	(x^2-y^2,xy)
A_{1u}	1	1	1	1	1	1	-1	-1	-1	-1	-1	-1	–	–
A_{2u}	1	1	1	1	-1	-1	-1	-1	-1	-1	1	1	z	–
B_{1u}	1	-1	1	-1	1	-1	-1	1	-1	1	-1	1	–	–
B_{2u}	1	-1	1	-1	-1	1	-1	1	-1	1	1	-1	–	–
E_{1u}	2	1	-1	-2	0	0	-2	-1	1	2	0	0	(x,y)	–
E_{2u}	2	-1	-1	2	0	0	-2	1	1	-2	0	0	–	–

Table A.6: Character table of D_{6h}^4 [51].

Bibliography

[1] H. L. Yakel, W. C. Koehler, E. F. Bertaut and E. F. Forrat. Acta Crystallogr **16**, 957, (1963).

[2] M. A. Gilleo. Acta Crystallogr **10**, 161, (1957).

[3] V. E Wood, A.E. Austin, E. W. Collings and K. C. Brog. J. Phys. Chem. Solids **34**, 859, 1973.

[4] A. Waintal and J. Chenavas. Compt. Rend B**168**, 264, (1967).

[5] D. L. Rousseau, R. P. Bauman and S. P. S. Porto. Journal of Raman Spectroscopy **10**, 253, (1981).

[6] D. G. Tomuta, S. Ramakrishnan, G. J. Nieuwenhuys and J. A. Mydosh. J. Phys. Condens. Matter **13**, 4543, (2001).

[7] Z. J. Huang, Y. Cao, Y. Y. Sun, Y. Y. Xue and C. W. Chu. Phys. Rev. B **56**, 2623, (1997).

[8] M. N. Iliev, H. G. Lee, V. N. Popov, M. V. Abrashev and A. Hamed, R. L. Meng and C. W. Chu. Phys. Rev. B **56**, 2488, (1997).

[9] A. Filippetti and N. A. Hill. J. Magn. Magn. Mater. **236**, 176, (2002).

[10] A. B. Souchkov, J. R. Simpson, M. Quijada, H. Ishibashi, N. Hur, J. S. Ahn, A. W. Cheong, A. J. Millis and H. D. Drew. Phys. Rev. Lett. **91**, 027203, (2003).

[11] B. Lorenz, A. P. Litvinchuk, M. M. Gospodinov and C. W. Chu. Phys. Rev. Lett. **92**, 087204, (2004).

[12] A. P. Litvinchuk, M. N. Iliev, V. N. Popov and M. M. Gospodinov. J. Phys. Condens. Matter **16**, 809, (2004)

[13] A. Munoz, J. A. Alonso, M. T. Casais, M. J. Martinez-Lope, J. L. Martinez and M. T. Fernandez-Diaz. J.Phys. Condens. Matter **14**, 3285, (2002).

[14] M. Fiebig and Th. Lottermoser. J. Appl. Phys. **93**, 8194, (2003).

[15] Th. Lottermoser, M. Fiebig, D. Frohlich, St. Leute and K. Kohn. J. Magn. Magn. Mater. **226**, 1131, (2001).

[16] M. Fiebig, D. Frohlich, K. Kohn, St. Leute, Th. Lottermoser, V. V. Pavlov and R. V. Pisarev. Phys. Rev. Lett. **84**, 5620, (2000).

[17] C. Degenhardt, M. Fiebig, D. Frohlich, Th. Lottermoser, and R. V. Pisarev. Appl. Phys. B **73**, 139, (2001).

[18] Th. Lottermoser, Th. Lonkai, U. Amann, D. Hohlwein, J. Ihringer and M. Fiebig. Nature **430**, 541, (2004).

[19] Hisashi Sugie, Nobuyuki Iwata and Kay Kohn. J. Phys. Soc. Jpn. **71**, 1558, (2002).

[20] M. Fiebig, C. Degenhardt and R. V. Pisarev. Phys. Rev. Lett. **88**, 027203, (2002).

[21] M. Fiebig, C. Degenhardt and R. V. Pisarev. J. Appl. Phys. **91**, 8867, (2002).

[22] Th. Lonkai, D. Hohlwein, J. Ihringer and W. Prandl. Appl. Phys. A **74**, S843, (2002).

[23] T. J. Sato, S. H. Lee, T. Katsufuji, M. Park, J. R. D. Coply and H. Takagi. Phys. Rev. B **68**, 014432, (2003).

[24] T. Katsufuji, S. Mori, M. Masaki, Y. Moritomo, N. Yamamoto and H. Takagi. Phys. Rev. B **64**, 104419, (2001).

[25] Bas B, Van Aken, Auke Meetsma and Thomas T. S. Palstra. Acta Crystallogr. C **57**, 230, (2001).

[26] Th. Lottermoser, M. Fiebig and D. Frohlich. J. Appl. Phys. **91**, 8251, (2002).

[27] A. Munoz, J. A. Alonso, M. J. Martinez-Lope, M. T. Casais, J. L. Martinez and M. T. Fernandez-Diaz. Phys. Rev. B **62**, 9498, (2000).

[28] J. F. Ackerman, G. M. Cole and S. L. Holt. Inorg. Chimica Acta **8**, 323, (1974).

[29] Sinclair. ISIS Experimental Report **8738**, (1998).

[30] D. Visser, G. C. Verschoor and D. J. W. Ijdo. Acta Crystallogr. **B36**, 28, (1980).

[31] O. A. Petrenko, M. A. Lumsden, M. D. Lumsden and M. F. Collins. J. Phys. Condens. Matter **8**, 10899, (1996).

[32] J. M. Perez-Mato, J. L. Manes, M. J. Tello and F. J. Zuniga. J. Phys. C: Solid State Phys. **14**, 1121, (1981).

[33] T. Kato, K. Machida, T. Ishii, K. Iio and T. Mitsui. Phys. Rev. B **50**, 13039, (1994).

[34] J. L. Manes, M. J. Tello and J. M. Perez-Mato. Phys. Rev. B **26**, 250, (1982).

[35] Z. W. Hendrikse, W. J. A. Maaskant. Physica. B **233**, 139, (1997).

[36] H. Tanaka and K. Kakurai. J. Phys. Soc. Jpn. **63**, 3412, (1994).

[37] T. Kato, T. Ishii, Y. Ajiro, T. Asano and S. Kawano. J. Phys. Soc. Jpn. **62**, 3384, (1993).

[38] Y. Nishiwaki, K. Ilo and T. Mitsui. J. Phys. Soc. Jpn. **72**, 2608, (2003).

[39] H. Yamaguchi, H. Uwe, T. Sakudo and E. Sawaguchi. J. Phys. Soc. Jpn. **57**, 147, (1988).

[40] H. Yamaguchi, H. Uwe, T. Sakudo and E. Sawaguchi. J. Phys. Soc. Jpn. **56**, 589, (1987).

[41] M. Yamaguchi, K. Inoue, T. Yagi, and Y. Akishige. Phys. Rev. Lett. **74**, 2126, (1995).

[42] K. Inoue, A. Hasegawa, K. Watanabe, H. Yamaguchi, H. Uwe, T. Sakudo. Phys. Rev. B **38**, 6352, (1988).

[43] A. Yamanaka and K. Inoue. J. Phys. Soc. Jpn. **66**, 3277, (1997).

[44] K. Inoue, A. Yamanaka, A. Hasegawa and H. Yamaguchi. Ferroelectrics **156**, 297, (1994).

[45] Y. Akishige, H. Takahashi, N. Mori and E. Sawaguchi. J. Phys. Soc. Jpn. **63**, 1590, (1994).

[46] Y. Ishibashi. J. Phys. Soc. Jpn. **63**, 1396, (1994).

[47] A. Yamanaka, K. Inoue, T. Furutani, J. Kawamata and H. Yamaguchi. Ferroelectrics **159**, 79, (1994).

[48] Y. Ishibashi and M. Tomatsu. J. Phys. Soc. Jpn. **58**, 1058, (1989).

[49] K. Inoue, A. Hasegawa, K. Watanabe, H. Yamaguchi, H. Uwe and T. Sakudo. Ferroelectrics. **135**, 6352, (1992).

[50] A. W. Joshi. Elements of Group Theory for Physicist. John Willey and Sons, (1977).

[51] Michael Tinkham. Group Theory and Quantum Mechanics. McGraw-Hill Book Company, (1964).

[52] R. S. Mulliken. Phys. Rev **43**, 279, (1933).

[53] C. J. Bradley and A. P. Cracknell. The Mathematical Theory of Symmetry in Solids. Clarendon Press, (1972).

[54] Theo Hahn. International Tables of X-Ray Crystallography. Kluwer Academic Publisher, (1996).

[55] Gerald Burns and A. M. Glazer. Space Groups for Solid State Scientists. Academic Press, (1990).

[56] G. F. Koster. Space Groups and Their Representations. Academic Press, (1957).

[57] J. Zak. The Irreducible Representations of Space Groups. W. A. Benjamin, (1969).

[58] O. V. Kovalev. Irreducible Representations of the Space Groups. Gordon and Breach Science Publishers, (1965).

[59] A. V. Shubnikov. Symmetry and Antisymmetry of Finite Figures. U. S. S. R. Academy of Sciences, Moscow, (1951).

[60] L. D. Landau. Collected Papers of Landau. Gordon and Breach Science Publishers, 1967.

[61] L. D. Landau and E. M. Lifshitz. Statistical Physics. Pergamon Press, 1980.

[62] Jean-Claude Toledano and Pierre Toledano. The Landau Theory of Phase Transitions. World Scientific, 1987.

[63] L. D. Landau. Zhurnal Eksperimental'noi i Fiziki **7**, 627, (1937).

[64] Pierre Toledano and Jean-Claude Toledano. Phys. Rev. B **14**, 3097, (1976).

[65] Pierre Toledano and Jean-Claude Toledano. Phys. Rev. B **16**, 386, (1977).

[66] Jean-Claude Toledano and Pierre Toledano. Phys. Rev. B **21**, 1139, (1980).

[67] Pierre Toledano and Jean-Claude Toledano. Phys. Rev. B **25**, 1946, (1982).

[68] Yu. M. Gufan. Sov. Phys. Solid. State **13**, 175, (1971).

[69] Yu. M. Gufan and V. P. Sakhnenko. Sov. Phys. JETP **36**, 1009, (1973).

[70] Yu. M. Gufan and V. P. Sakhnenko. Sov. Phys. Solid. State **16**, 1034, (1974).

[71] Yu. M. Gufan. Structural Phase Transitions. Nauka, Moscow, (1982).

[72] E. I. Kutin, V. L. Lorman and S. V. Pavlov. Sov. Phys.Usp **34**, 497, (1991).

[73] Pierre Toledano and Vladimir Dmitriev. Reconstructive Phase Transitions. World Scientific, (1996).